General Disclaimer

One or more of the Following Statements may affect this Document

- This document has been reproduced from the best copy furnished by the organizational source. It is being released in the interest of making available as much information as possible.

- This document may contain data, which exceeds the sheet parameters. It was furnished in this condition by the organizational source and is the best copy available.

- This document may contain tone-on-tone or color graphs, charts and/or pictures, which have been reproduced in black and white.

- This document is paginated as submitted by the original source.

- Portions of this document are not fully legible due to the historical nature of some of the material. However, it is the best reproduction available from the original submission.

PLASMA PHYSICS GROUP

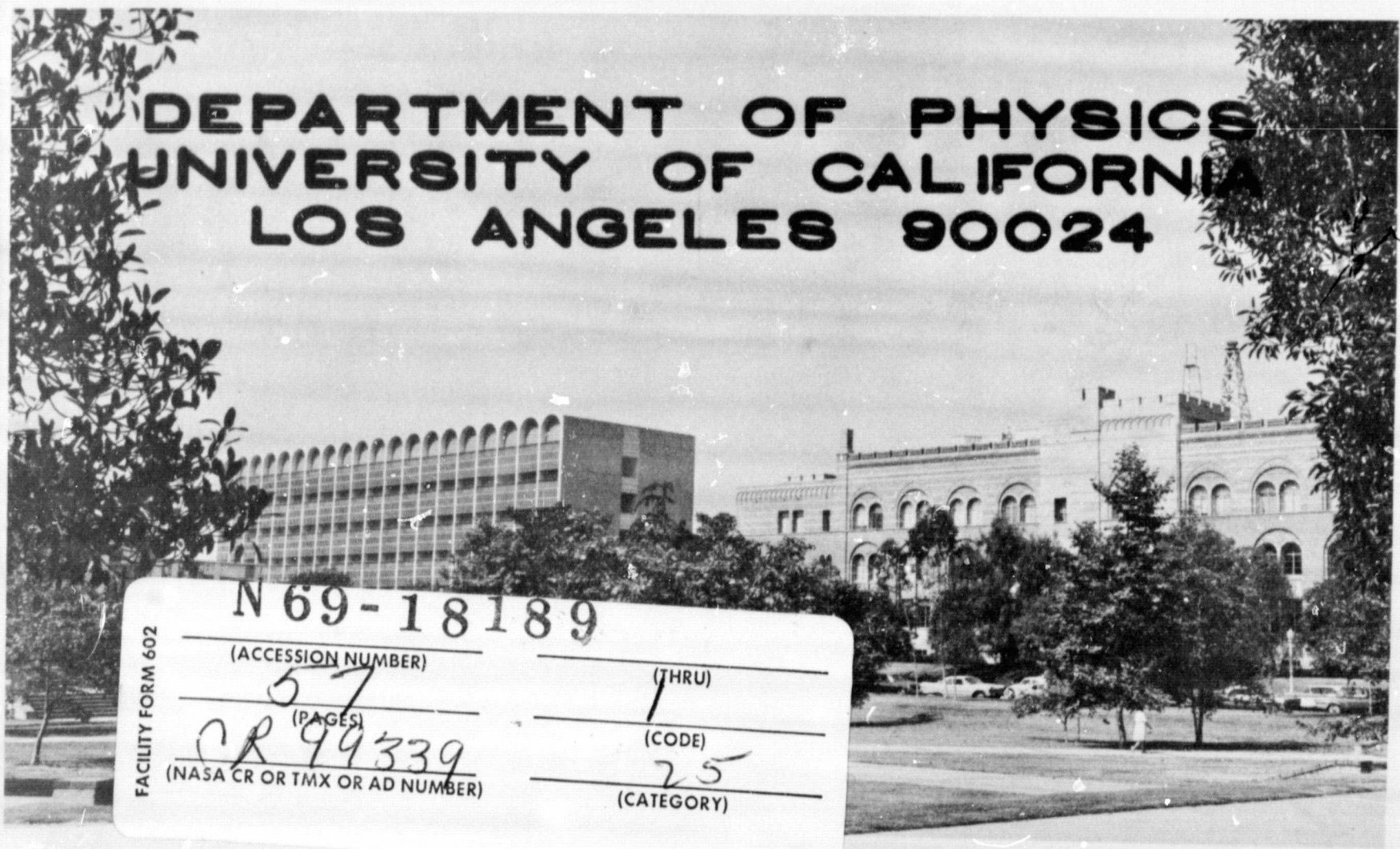

Drift Waves in the Linear Regime

R. E. Rowberg and A. Y. Wong

February, 1969 R-39

Plasma Physics Group
Department of Physics
University of California
Los Angeles, California 90024

This research was supported by funds from NASA Grant No. NGR-05-007-066.

Drift Waves in the Linear Regime

R. E. Rowberg and A. Y. Wong

Department of Physics, University of California, Los Angeles, California

ABSTRACT

A method of external excitation of density gradient drift waves in a stable, collision dominated plasma is presented whereby the linear theory of drift waves is verified. The procedure permits limitation of the perturbation amplitude such that $e\phi_1/kT < 0.1$. This represents a marked advance in the study of drift waves since non-linear saturation effects present in all previous experiments on these waves are avoided. The driven oscillations are coherent, nearly sinusoidal modes on which measurements of ω and $\underline{k}$ as a function of the plasma parameters are made. In this manner the linear dispersion relation derived from the fluid equations is verified demonstrating the strong stabilizing effect of transverse diffusion resulting from ion viscosity. In connection with this an additional damping process resulting from ion loss at the cathodes is introduced whereby complete stabilization of the plasma to drift waves is possible. Next, the dependence of the growth rate on the phase angle between the density and potential perturbation is shown in the regime where viscous damping is not dominant. Finally verification of the dependence of the axial wavelength on the sheath conditions at the plasma cathode boundary and on the length of the plasma column is demonstrated.

I. INTRODUCTION

A. Scope

In this work we report on a method of investigating the linear behavior of drift waves in a collision dominated plasma. Taking advantage of the fact that drift waves can be stabilized in a bounded plasma such as in a Q-device, we are able to externally excite these oscillations and study their characteristics. The method on external excitation has the advantage that we are able to look at small amplitude waves ($\frac{e\phi}{KT} < 0.1$) wherein non-linear processes have a negligible effect on the behavior of these oscillations. This is not the case in the unstable regime where all previous investigations of drift waves have taken place. Consequently, our method of study represents a marked advance in analyzing the behavior of these waves.

B. Basic Description of Drift Waves

In as inhomogeneous plasma immersed in a magnetic field, B, there are waves associated with density and temperature gradients. Such waves are low frequency, electrostatic oscillations which propagate almost perpendicular to both B and the gradients. This perpendicular propagation is in the direction of the electron diamagnetic drift and the phase velocity of the wave is approximately that of this drift. These "drift" waves also propagate in the axial direction (parallel to B) and possess a very long longitudinal wavelength, λ_z . For a plasma bounded in the axial direction these oscillations reflect off the ends and form standing waves with the boundary conditions determining λ_z.

In a plasma dominated by collisions, the drift wave is normally unstable as a result of finite ion inertia, finite Larmor radius effects, and electron-ion collisions. There three effects combine with the zero

order density gradient to cause any initial drift wave-like perturbation to grow in amplitude. In addition there are damping processes which can stabilize the plasma. One such mechanism is ion-ion collisions which diffuses the density perturbation transverse to B. Another damping mechanism which can exist occurs when the plasma is bounded axially such as in a Q-device. This process is due to ion loss at these bounding end plates. Under certain conditions, to be discussed below, these two mechanisms can combine to stabilize the plasma against drift waves. It is in this regime that the experiment described below is performed.

Drift waves belong to a class of microinstabilities which have received a great deal of attention in recent years. This is because they can occur in all plasmas which are not in equilibrium as is the case with confined plasmas. The drift instability in particular is a result of the density gradient inherent to a confined plasma. Of further importance is that this instability is suspected of being one of the mechanisms responsible for the anomalous diffusion observed in controlled fusion devices, e.g. stellerator pumpout.[1] The reason for this is that there is a net radial transport of particles outward arising from the fluctuating electric field of unstable drift waves. Diffusion rates calculated from diffusion processes resulting from these waves are much larger than those of classical diffusion.[1,2,3] In addition recent experiments have shown that enhanced diffusion takes place when drift waves are present.[3,4] For these reasons a basic understanding of the drift wave is essential to the problem of plasma confinement.

C. Historical Development

Early theoretical work on drift waves dealt with the collision-

less (electron-ion collisions neglected) limit. Such work is described in articles by Rudakov and Sagdeev (1960),[5] Kadometsev and Timofeev (1962)[6] and Rosenbluth and Krall (1963).[7,8] These works involved drift instabilities excited by density and temperature gradients. The first work on collisional plasmas was performed by Sagdeev and Moiseev (1963)[9] and Chen (1964 and 1965).[10] Their treatment consisted of solving the fluid equations for drift waves driven by density gradients. Coppi (1967)[11] extended this work by including ion-ion collisions demonstrating that such collisions have a stabilizing effect on the drift wave.

Several experimental observations of drift wave like oscillations in thermally ionized Cs or K plasmas were made by D'Angelo and Motley (1963),[12] Lashinsky (1964),[13] and Buchelnikova (1964)[14] among others. However while these waves had characteristics in common with those predicted for density gradient drift waves, Hendel[3] has pointed out that certain discrepancies appear in these observations which make identification of these oscillations as this type of drift wave difficult. The first positive identification of density gradient drift waves was made by Hendel, Chu and Poletzer (1967).[3] Their work verified the theoretical work of Coppi regarding the stabilization of drift waves by ion viscosity.

The experiment to be described in this paper also makes positive identification of the density gradient drift wave and demonstrates the important contribution of ion viscosity. However, unlike the experiments just described which involved unstable drift waves and consequently non-linear processes, we are able to perform our experiment in the linear regime by use of the technique of external excitation of these oscillations which allows us to limit the perturbation amplitude to $e\phi_1/KT < 0.1$. We can therefore use this procedure for the verification

of the linear dispersion relation as in the case of ion acoustic waves.[15] The principal points checked for the drift waves in this manner are the real and imaginary frequencies, the phase angle between the density and potential perturbations, and the axial wavelength. Similar excitation techniques have also been used by Hai and Wong (1968)[16] for the investigation of large amplitude drift waves.

In section II we present the linear the theory of drift waves deriving a dispersion relation and expressions for the real and imaginary frequencies. We then obtain as expression for the phase angle between the density and potential perturbations. Finally we derive an expression for end plate damping based on ion recombination at the cathodes. This shows that under certain experimental conditions end plate damping can stabilize the drift wave. Section III contains a description of the experimental apparatus and procedure. Finally in Section IV we present the experimental results and compare these results to those theoretically predicted.

II. THEORY

We wish to calculate a dispersion relation for the density gradient drift wave. Following the procedure of Chen[10] and Hendel, Chu, and Politzer[3] we solve the linearized fluid equations in a rectangular geometry for a magnetically confined, inhomogeneous plasma. Such a system is displayed in Figure 1. We then obtain expressions for the axial wavelength of the drift wave as a function of plasma parameters, the phase angle between the density and potential perturbations, and the damping rate due to ion loss at the end plates.

In order to perform the calculation we make the following assumptions:

(1). We may use the fluid equations since $\omega << \omega_c, \nu_{ei}$ where ν_{ei} is the electron-ion collision frequency, ω_c is the ion cyclotron frequency , and ω is the drift wave frequency.

(2). $\frac{8\pi n_o kT}{B^2} << 1$ so that $\underline{E}_1 = -\nabla \phi_1$. Here n_o kT and $B^2/8\pi$ are the thermal and magnetic energies and $\underline{E}_1$ is the perturbed electric field. n_o, T, and B are the zero order density, temperature, and magnetic field.

(3). The axial magnetic field (along z) is uniform and constant.

(4). Axial ion motion and variation are neglected since $\frac{\omega}{k_z} >> v_{ith}$ where v_{ith} is the ion thermal velocity.

(5). Electron inertia is neglected.

(6). $k_\perp$, $k_z << k_D$ so that we may assume quasi-neutrality. $k_\perp$, k_z, and k_D are the perpendicular (to B), parallel, and Debeye wave numbers.

(7). There is a zero density gradient in the negative x direction

(Figure 1) ($\frac{dn_o}{dx}$) and $\frac{1}{n_o}\frac{dn_o}{dx}$ is constant.

(8). All first order quantities vary as $\exp[-i(\omega t - k_x x - k_y y - k_z z)]$. This implies that $k_x > n_o'/n_o$, the density gradient scale length, so that the wave is localized in the x direction.

(9). $\frac{\omega}{k_z}$, $\frac{\omega}{k_\perp} << v_{eth}$ so that the temperature is constant. In addition T is the same for both ions and electrons. $v_{eth} = kT/m_e$, the electron thermal velocity.

The fluid equations for our system can be written down as follows:

$$(1) \qquad Mn\left(\frac{\partial \underline{v}_\perp}{\partial t} + \underline{v}_\perp \cdot \nabla_\perp \underline{v}_\perp\right) = nq\left[\underline{E}_\perp + \frac{\underline{v}_\perp \times \underline{B}}{c}\right] - \nabla_\perp p - \nabla_\perp : \underline{\underline{\Pi}} = 0$$

for electrons (q=-e, M=0) and ions (q=+e) perpendicular to the magnetic field,

$$(2) \qquad 0 = ne E_z + \nabla_z p + n m_e \nu_{ei} \underline{v}_z$$

for electrons parallel to B, and

$$(3) \qquad \frac{\partial n}{\partial t} + \nabla \cdot (n \underline{v}) = 0$$

the continuity equation. n and v are equal to $n_1 + n_o$ and $v_1 + v_o$ respectively where the subscript 1 indicates perturbed quantities and o indicates zero order quantities, p is the scalar pressure and is equal to nkT, $\underline{\underline{\Pi}}$ is the pressure tensor (ions only), and ν_{ei} is the electron-ion collision frequency. For the zero order steady state motion Eq. (1) is solved to give

$$(4) \qquad V_{oye} = -\frac{KT}{eB}\frac{1}{n_o}\frac{dn_o}{dx} = -V_{oy} \equiv V_D$$

the electron and ion diamagnetic drifts.

To solve for the first order motion we linearize Eqs. (1) and (2) using the form of $\underline{\underline{\Pi}}$ given by Shkarofsky, Bernstein, and Robinson,[17] with the simplification[3] that the collisional term is given by $\frac{1}{q}\frac{n_e kT}{\omega_c^2}\nu_{ii}\nabla_\perp^2 \underline{v}_\perp$, and Eq. (4) for the zero order velocity arising in the $\underline{v}_\perp\cdot\nabla_\perp\underline{v}_\perp$ term. Using the assumptions listed we solve for the first order velocities and substitute them into the linearized continuity equations for ions and electrons. Making the approximations $(\nu_{ii}/\omega_c) << 1$ and wave localization in the x direction the terms involving $k_x(n_o'/n_o)$ and (ν_{ii}/ω_c) can be dropped. The approximations are valid experimentally although the localization condition holds well only for mode number ≥ 2. As a result of this procedure we obtain

$$(5)\quad \omega\frac{n_i}{n_o} - k_y v_D\frac{e\phi_1}{kT} + b\omega\frac{e\phi_1}{kT} + bk_y v_D\frac{e\phi_1}{kT} + i\frac{1}{t_\perp}\left(\frac{n_i}{n_o} + \frac{e\phi_1}{kT}\right) = 0$$

for ions, and

$$(6)\quad \omega\frac{n_{ic}}{n_o} - k_y v_D\frac{e\phi_1}{kT} + i\frac{1}{t_{11}}\left(\frac{n_{ic}}{n_o} - \frac{e\phi_1}{kT}\right) = 0$$

for electrons. Here we have defined $b = (k_\perp \rho_i)^2$, where $k_\perp^2 = k_x^2 + k_y^2$ and ρ_i is the ion cyclotron radius, $(t_\perp)^{-1} = \frac{1}{4} b^2\nu_{ii}$, where ν_{ii} is the ion-ion collision frequency, and $(t_{11})^{-1} = k_z^2 v_{eth}^2/\nu_{ei}$. Solving Eqs. (5) and (6) for n_i'/n_o respectively and equating gives us the dispersion relation for collisional drift waves. This is

$$(7)\quad \omega^2 b + \omega\left[bk_y v_D + i\left(\frac{1}{t_{11}}(1+b) + \frac{1}{t_\perp}\right)\right] - ik_y v_D\left[\frac{1}{t_{11}}(1-b) - \frac{1}{t_\perp}\right] - \frac{2}{t_{11}t_\perp} = 0.$$

This equation is identical fo that derived by Dupree[2] using a kinectic approach and nearly the same as the one derived by Hendel, Chu, and Politzer.[3] Further in the limit $t_\perp \to \infty$ and $b \ll 1$ Eq. (7) reduces to that obtained by Chen.[10] Eq. (7) is in general solved numerically. However by expanding the square root in the limit $b^2 \ll 1$ and $t_{11}^{-1} \ll k_y v_D$ (the latter condition allows us to drop the last term in Eq. (7)) we can obtain approximate forms for the real frequency (ω_R) and growth rate (ω_g) which demonstrates the physics involved. These are

$$\omega_R = \frac{k_y v_D \left[1 - b - \frac{t_{11}}{t_\perp}\right]}{\left[1 + b + \frac{t_{11}}{t_\perp}\right]} \tag{8}$$

$$\omega_g = \frac{2(k_y v_D)^2 b\, t_{11} \left[1 - b - \frac{t_{11}}{t_\perp}\right]}{\left[1 + b + \frac{t_{11}}{t_\perp}\right]^3} \tag{9}$$

In the limit $b \ll 1$ and $t_\perp \to \infty$ we recover the expressions derived by Chen[10]

$$\omega_g = 2(k_y v_D)^2 b\, t_{11} \quad , \quad \omega_R = k_y v_D \tag{10}$$

In this limit the growth rate is due to a phase shift between the density and potential perturbation.[10] This puts a component of the first order ion motion in the x direction in phase with the density perturbation causing n_1 to increase in magnitude. If we now introduce ion viscosity through finite Larmor radius (FLR) effects and ion-ion collisions (i.e. keeping terms involving b and $t_\perp$) a stabilizing mechanism is provided[3] which permits ω_g to become ≤ 0. This is a result of

diffusion across $(k_\perp)^{-1}$ generated by the viscous forces arising from FLR and ion-ion collisions. Such diffusion causes the wave to diminish in amplitude. Eq.(9) shows that stabilization ($\omega_g=0$) occurs when $t_{ii} = t_\perp(1-b)$. $t_\perp$ is the time it takes the ions to diffuse across $(k_\perp)^{-1}$ by way of ion-ion collisions. The 1-b correction means that the FLR reduces the distance and therefore the effective time required for the viscous diffusion to take place. This correction arises from the terms (1+b) and (1-b) in the dispersion relation, Eq.(7). Similar terms are present in the dispersion relation derived by Hendel, Chu and Politzer[3] but were not considered in the stability analysis. The significance of t_{ii} is that it is the time required for the perturbed electron fluid to expand along the field lines against electron-ion collisions over a distance $(k_z)^{-1}$ thereby establishing the perturbed potential, ϕ_1. ϕ_1 in turn generates the x motion of ions necessary for the wave to propagate and grow. Therefore stability is achieved if the transverse diffusion time due to FLR and ion-ion collisions is equal to or less than the electron expansion time. This situation results in a decayed perturbation before ϕ_1 can be set-up. As we increase the magnetic field from the stability point, $t_\perp(1-b)$ becomes greater than t_{ii} and the growth rate is positive and increasing. The latter is a result of the increase in the term in Eq.(9) containing viscous effects, $[1-b-t_{ii}/t_\perp]$, being dominant over the decrease in the portion of ω_g (Eq.(9)) resulting from the $n_1 - \phi_1$ phase shift (Eq.(10)). The approximate range of values of the viscous term where this takes place is $0 \leq [1-b-t_{ii}/t_\perp] \leq 0.5$. Beyond this the portion of ω_g due to the phase shift becomes dominant and ω_g decreases with increasing B. Therefore the growth rate shows a maximum at some intermediate value of B.

Stabilization also occurs at very small values of t_{ii} ($t_{ii}^{-1} >> k_y v_D$) even though $t_{ii} << t_\perp(1-b)$. In this case a small t_{ii} means a small $n_1 - \phi_1$

phase angle and a small resultant growth mechanism.[10] If we decrease $t_{\parallel}$ for a fixed value of $t_{\perp}$ a point will be reached where the growth rate due fo the the $n_1 - \phi_1$ phase angle (Eq. (10)) becomes less than the transverse diffusion rate due to ion viscosity and the wave damps out.[3] This process can be expressed quantitatively by keeping the term $2/t_{\parallel} t_{\perp}$ in Eq. (7) and solving this equation in the limit $b << 1$ and $t_{\parallel} << t_{\perp}$. The approximate growth rate becomes[10]

$$\omega_g = 2(k_y v_D)^2 b t_{\parallel} \left[1 - \frac{1}{b(k_y v_D)^2 t_{\parallel} t_{\perp}} \right] \tag{11}$$

Therefore $\omega_g = 0$ when $t_{\perp} = [b(k_y v_D)^2 t_{\parallel}]^{-1}$. The right side of this equation is just the growth time due to the $n_1 - \phi_1$ phase shift as seen from Eq. (10). Since both sides of this expression vary as n_o, $(B)^4$, and $(m)^4$, only k_z remains as a variable. In the experiment under study $t_{\parallel}$ lies between the limiting cases presented and consequently both stabilizing processes must be included. When this is done the approximate expression for ω_g becomes

$$\omega_g = \frac{2(k_y v_D)^2 b t_{\parallel}}{\left(1 + b + \frac{t_{\parallel}}{t_{\perp}}\right)} \left[\frac{\left(1 - b - \frac{t_{\parallel}}{t_{\perp}}\right)}{\left(1 + b + \frac{t_{\parallel}}{t_{\perp}}\right)^2} - \frac{1}{b(k_y v_D)^2 t_{\parallel} t_{\perp}} \right]. \tag{12}$$

The presence of the last term in the large bracket of Eq. (12) means that stability is achieved ($\omega_g = 0$) for values of $[1 - b - t_{\parallel}/t_{\perp}] > 0$. Moreover for the experimental conditions present the viscous portion of Eq. (12) dominates (i.e. ω_g increases with increasing magnetic field) for values of $[1 - b - t_{\parallel}/t_{\perp}]$ up to 0.7 which is a larger range than in the case where $t_{\parallel}^{-1} << k_y v_D$. Therefore we are in the viscous regime when

$[b+t_{\parallel}/t_{\perp}] \geq 0.3$ for our particular experiment.

With regard to k_z we wish to briefly discuss the effects of the sheaths of a thermally ionized plasma at the cathodes of a Q-device on determining the allowed values of k_z. Chen[18] has shown that the sheath structure has a pronounced effect on the effective axial wavelength, λ_z. For electron rich sheaths, which are good conductors, the perturbation is zero at the sheath edge and $\lambda_z \simeq 2L$ where L is the column length. Ion rich sheaths, on the other hand, provide an insulating boundary which permits a finite perturbation of the sheath-plasma boundary. Therefore $\lambda_z \gg 2L$ in this case. Chen[18] has derived an expression giving the allowed values of k_z based on the boundary and plasma conditions. This is

$$(13) \qquad \frac{K_z L}{2} \tan \frac{K_z L}{2} = \frac{L}{2\rho_i} \frac{\nu_{ei}}{\omega_c} \left(\frac{1}{2\pi} \frac{m_e}{M}\right)^{1/2} \begin{cases} 1 & U<0 \\ \exp[-eU/KT] & U>0 \end{cases}.$$

U is defined as the plasma potential with respect to the grounded cathodes. For $U < 0$ the sheaths are electron rich and for $U > 0$ they are ion rich. Eq. (13) is experimentally verified in section 4.

We next comment on the phase angle (Θ) between the density (n_1) and potential (ϕ_1) perturbations. As has been stated this angle is responsible for the growth mechanism of the drift waves.[10] We can derive an expression for Θ from Eqs. (5) and (6). By subtracting Eq. (6) from (5) and solving for n_1 in terms of ϕ_1, we can immediately write down for $\tan\Theta$

$$(14) \qquad \tan\Theta = -\frac{b(\omega_R + K_y V_D) t_{\parallel}}{1 + \frac{t_{\parallel}}{t_{\perp}} + b\omega_s t_{\parallel}}.$$

When $t_\perp \to \infty$ the expression becomes

$$(15) \qquad \tan\Theta = -2b(k_y v_b)t_{11} = -\frac{\omega_g}{k_y v_D}$$

where we have used Eq. (10) for ω_g. We note that in this limit ω_g varies directly with Θ. This is demonstrared experimentally in section 4.

In the viscous regime ($b+t_{11}/t_\perp > 0.3$), however, ω_g no longer varies directly with Θ. The principal contribution of ion viscosity to $\tan\Theta$ is to increase the value of ω_R as B increases (Eq. (8)). However both b and $k_y v_D$ decrease as B gets larger and therefore $\tan\Theta$ will be decreasing for this case (Eq. (14)). The growth rate, on the other hand, is increasing for the reasons discussed above (see Eq.(12)). Therefore when ion viscosity dominates the behavior of the drift wave the growth rate will increase even though Θ is decreasing. i.e. the principal effect of ion viscosity is to diffuse away the density perturbation and this process has little effect on the magnitude of the phase angle.

The final point we wish to discuss is the phenomenon of end plate damping.[18] This provides an additional damping mechanism independent of the drift wave processes just discussed. The damping is a result of ion loss at the bounding cathodes due to recombination. Depending on the sheath structure at these cathodes the loss rate can be large enough to stabilize the drift wave. This will occur when the sheaths are ion rich. Plasma ions are then able to easily escape to the cathodes but are hindered from returning by the potential barrier at the plasma-sheath boundary. Such circumstances increases the probability of recombination. Since recombined ions are replaced by ions formed from the neutral

beam the information contained in the perturbation is gradually lost. If the rate of ion loss to the cathodes is greater than any drift wave growth rate in the plasma, the plasma will be stable. A simple calculation derived in a manner suggested by Chen[19] will give us an expression for this damping rate.

The damping rate is defined as

$$\omega_D = \frac{1}{N_1}\frac{\partial N_1}{\partial t} \tag{16}$$

where $N_1 = Ln_1$ is the total number of perturbed ions per unit area in the plasma column of length L and $\partial N_1/\partial t$ is the rate at which these ions are lost to the cathodes. For ion rich sheaths a flux $J_1 = 2[n_1 v_{ith} + n_o v_{1z}]$ is incident of the two cathodes. v_{1z} is the perturbed ion velocity along z and v_{ith} is the ion thermal velocity. Since $v_{1z} << v_{ith}$ we neglect the term containing v_{1z}.[10] On the first bounce off the cathode a fraction $(1-p)J_1$ is lost due fo recombination. p is the probability of ionization and is defined as[20]

$$P = \frac{La(T)}{1 + La(T)} \tag{17}$$

where $La(T) = \exp[(U_W - U_I)/kT]$ is the Langmuir-Saha equation. U_W is the work function of the cathode and U_I is the ionization potential of the neutrals. The current not recombined, pJ_1, is reflected back toward the plasma where a fraction $J_1\ p\ \exp[-eU/kT]$ $(U > 0$, ion sheath) escapes the sheath. The current not escaping $(1-\exp[-eU/kT])pJ_1$ is reflected back to the cathode whereupon a fraction $(1-p)(1-\exp[-eU/kT])pJ_1$ is lost. This process continues and $\partial N/\partial t$ is just the sum over all bounces of the loss at each bounce. We than have

$$\frac{\partial N_i}{\partial t} = \frac{(1-p)\,J_i}{[1-p(1-\exp[-eU/kT])]} \tag{18}$$

where we have assumed an infinite number of bounces. This is justified since the transit time for an ion in the sheath is several orders of magnitude less than the drift wave growth time. Substituting Eqs. (17), (18), and the expression for N_i into Eq. (16) we obtain

$$\omega_D = \frac{2\,v_{ith}}{L}\,\frac{1}{1+La(T)\exp[-eU/kT]} \tag{19}$$

as the damping rate in the presence of ion sheaths. A similar calculation for electron rich sheaths yields

$$\omega_D = \frac{2\,v_{ith}}{L}\,\frac{\exp[eU/kT]}{1+La(T)}\,,\quad U<0\,. \tag{20}$$

This expression is much smaller because of the exp[eU/kT] in the numerator. Consequently end plate damping is largest in the case of strong ion sheaths and smallest in the case of electron sheaths.

We note that Eq. (19) is insensitive to changes in the magnetic field and inversly proportional to variation in the length of the plasma column. In the experiment we necessarily measure the net damping of the drift wave which is a combination of the linear growth rate and the end plate damping. The net damping will vary through the growth rate only since ω_D does not change with field whereas variation of the column length causes change in both the growth rate and end plate damping rate.

III. EXPERIMENTAL SET-UP

A. Apparatus

The experiment is performed on a Q-device[21] which produces a quiescent, highly ionized (40-90%) K or Cs plasma. The plasma is formed by contact ionization of K or Cs atoms from an atomic beam on the surface of a hot tungsten plate ($\sim$ 2200°K) and thermionic emission of electrons by the plate. The plasma is in thermodynamic equilibrium with the hot cathodes and is at a temperature of 0.2 ev. By varying the flux in the atomic beam we can vary the plasma density from 10^9 to 10^{12} cm^{-3}. The plasma forms a cylindrical column with a diameter of 5.8 cm and a nominal column length of 60 cm. It is radially confined by an axial magnetic field which is continuously variable from 0 to 4200 gauss. In addition our machine has the unique feature that the length of the plasma column can be varied during operation. This is accomplished by mounting the cathode assembly on vacuum sealed bellows placed at the ends on the vacuum chamber. A total variation of the column length of 25 cm is possible with the bellows.

B. Preliminary Adjustments

Certain conditions must be achieved in order to perform the experiment. First of all the effects of large temperature gradients ($T'/T \sim 1\ cm^{-1}$) must be considered in performing this experiment. It is necessary to separate the regions of large temperature and density gradient ($T'/T \sim n_o'/n_o \sim 1\ cm^{-1}$) in order to avoid confusion between density gradient drift waves and those excited by temperature gradients and their associated electric fields. In our experiment this is achiev-

ed by using a large tungsten ionizer plate (5.8 cm in diameter) so that the neutral flux falls will inside the edge of the plate. This results in a small temperature gradient where the density gradient is large (i.e. $T'/T \sim n_o'/n_o \sim 1\ cm^{-1}$) and a separation of the two types of oscillations as seen in Figure 2.

It is also necessary that the probes and cathodes be aligned relative to the magnetic field so that the measurement of position dependent quantities are accurate. By use of narrow electron and laser beams we can achieve alignment to within one mm. This is verified by our floating potential profiles which demonstrates that the measured profiles are within one mm of the diameter of the cathodes.

C. Experimental Procedure

The plasma is first stabilized against drift oscillations by a combination of end plate damping and ion viscous damping. We are then able to generate the drift wave by applying an external signal at the appropriate frequency to a grid [22] inserted radially into the plasma (Figure 3). The signal source is an audio oscillator and the signal amplitude of the driver is maintained so that $e\phi_1/kT<0.1$. This allows us to remain in the linear regime. The excitation grid is maintained at floating potential by inserting a capacitor (1.0μf) between the grid and the oscillator. This means that no steady state current is drawn by the grid. The grid is a 1.5x1.5 cm wire mesh constructed of 0.0025 cm Ta wire with 20 lines per cm. The wire mesh requires no frame to keep it rigid thus minimizing the perturbing

Influence on the plasma. The plane of the grid is oriented parallel to the magnetic field. The grid lead which also supports the wire mesh is 0.025 cm Ta wire which is electrostatically shielded so as to insure that excitation takes place only at the grid. The oscillation is received by a shielded Langmuir probe which is either biased at the ion saturation point to observe n_1 or floated to observe ϕ_1. With regard to the latter it is necessary to avoid the instrument phase shifts brought about by the stray capacitance of the receiving network and the load resistance (R_L) of the probe. Since the latter changes from 3×10^5 ohms when the probe is floating to 5×10^3 ohms when it is biased there will be a large phase shift introduced between n_1 and ϕ_1 by the receiving networks. This is eliminated by using a "bootstrap" technique to eliminate the capacitive loading of the floating probe.[23] Using a unity gain operational amplifier with input impedence of 3×10^7 ohms and 2pf for the measurement of ϕ_1, we are able to reduce the system phase shift between n_1 and ϕ_1 to less than 1°.

The probe signal is observed on an oscilloscope and a wave analyzer (Figure 3). By using the analyzer as the driving source in its tracking generator mode, we can measure the frequency response directly as we sweep the oscillator. This permits direct measurement of the resonant or real frequency of the drift wave. In order to measure the imaginary frequency we insert a tone burst generator between the oscillator and the excitation grid (Figure 3). We set the gate of the tone burst to allow enough oscillations through to establish a steady state wave in the plasma. The driving signal is then removed and the subsequent damping of the wave is observed on the scope

(Figure 3). The damping rate measured in this manner is a combination of the end plate damping and the linear growth rates.

Radial potential, density, and wave amplitude profiles are measured by motorized Langmuir probes which permits direct display of these profiles on an X-Y recorder. A set of typical profiles is displayed in Figure 2. Axial wave variation is measured by Langmuir probes which move along the field lines. These probes can rotate in the cross sectional plane of the plasma.

IV. EXPERIMENTAL RESULTS

In this section the experimental results are presented. We begin by discussing the qualitative features which identify the density gradient drift wave. A more detailed discussion of the axial wavelength follows comparing the experimental results to the theoretical predictions. Next, verification of the linear dispersion relation is presented with measurement of the real frequency and growth rate as a function of both the magnetic field and the plasma column length. Finally we present measurements of the phase angle between the density and potential perturbations and compare them to their corresponding growth rates.

A. Qualitative Features

There are several qualitative features of density gradient drift waves which are readily observed. These include both the predicted characteristics which identify the drift wave as well as features connected with the phenomenon of external excitation of these waves.

The externally excited drift wave appears as almost sinusoidal, single modes. The wave is observed to propagate in the azimuthal direction parallel to the electron diamagnetic drift. The azimuthal wave number (corresponding to k_y) is fixed by the periodicity requirement as m/r_o where m is the mode number and r_o is the position of the maximum of the radial wave amplitude measured from the plasma center. The mode number is determined by measuring the phase shift between Langmuir probes displaced azimuthally by 90° intervals. r_o ranges from 1.4 to 1.8 cm. A typical wave profile is shown in Figure 2 (inner wave profile (I)). Measurement of the profile width shows that k_r ($\sim k_x$) is approxi-

mately equal to k_θ ($\sim k_y$). In addition we note that the behavior of the excited waves in the stable regime goes over smoothly to that in the unstable regime with regard to these characteristics.

The outer wave profile (2) displayed in Figure 2 is the temperature gradient drift wave mentioned in section 3. We observe that this oscillation possesses characteristics, with respect to frequency and propagation properties, which are very similar to those of the density gradient drift wave (1). Consequently positive identification of the latter can only result if the regimes where the two waves peak ($n_o'/n_o \sim 1cm^{-1}$ for (1) and $T'/T \sim 1cm^{-1}$ for (2)) are isolated from each other.

Measurement of the density (n_1/n_o) and potential ($e\phi_1/kT$) perturbations demonstrates that these two quantities are equal within 10% over the entire wave profile. The measurements of $e\phi_1/kT$ are taken with a Langmuir probe across a 30 megohm resistor to insure that the probe is floating. Additionally we observe that the maximum amplitude of the driven perturbation is less than 5% which is well within the linear regime. This condition is maintained throughout the experiment.

Finally we wish to comment on the positioning of the excitation grid. We observe that maximum response is observed when the grid is at r_o. Moving it on either side of r_o reduces the amplitude of the received signal. In addition moving the position of the exciter in the axial or azimuthal directions at a fixed r_o does not change the characteristics of the received signal. To check on any possible stabilizing influence by the grid, it is periodically removed from the plasma to verify thet the plasma is stable. Measurements of density and

and potential profiles also show no detectable effects due to the presence of the grid.

B. Axial Wavelength

The axial wavelength of the drift wave is measured by moving a Langmuir probe parallel to the magnetic field at a fixed position in the r-Θ plane of the plasma. Since the drift wave is a standing wave in the axial direction the amplitude profile along z indicates the axial wavelength, λ_z. In this connection we observe no phase shift as we move along z verifying the standing wave nature. The results for two different plasma potential configurations are shown in Figure 5. The end plates are adjusted for equal temperatures so that negligible axial current flows. The plasma potential, U, is calculated in terms of the density and temperature according to[24]

$$U = \frac{KT}{e} \ln \left[\frac{4Ri(T)}{n_o e v_{e+h}} \right]$$

where Ri(T) is the Richardson-Dushman equation. We observe a flattening of the axial wave profile and consequently an increase in λ_z as we go from U = -0.05 volts (electron rich sheaths) to U = +0.50 volts (ion rich sheaths). These values of λ_z can be compared to the theoretically predicted values obtained from Eq. (13). Using the values of U given we find $\lambda_z \simeq 2L$ (L is the length of the plasma column) for U = -0.05 v and $\lambda_z \simeq 4L$ for U = +0.50 v. The theoretical curves drawn in Figure 5 are proportional to $\cos(k_z z)$ for the computed valued of k_z in the two cases. The agreement between theory and experiment demonstrates the dependence of λ_z on the end plate sheath conditions. In addition the dependence of the axial wavelength of L is measured. By

using the bellows assembly described in section 3, L is changed from 60 cm to 46 cm. For the case of electron rich sheaths we observe a change in the axial profile as displayed in Figure 6. Again the theoretical curves are calculated from Eq. (13) and the agreement between theory and experiment points out the dependence of k_z on L.

C. Variation of the Magnetic Field

Verification of the linear dispersion relation, Eq. (7), is performed by measuring the real frequency and growth rate as a function of both the magnetic field and plasma column length. In this part we examine the variation with the magnetic field.

The real frequency is easily measured by observing the resonant frequencies when exciting the drift waves. We have measured this frequency as a function of magnetic field. Results are displayed in Figure 7 for the m = 1, 2, and 3 modes. In order to make the results meaningful with respect to the dispersion relation, Eq. (7), we subtract the Doppler frequency due to the $\underline{E}_{or} \times \underline{B}$ drift from the data. The Doppler frequency is expressed as

$$\omega_{RE} = \frac{m}{r_o} \frac{c E_{or}}{B} \quad . \tag{21}$$

r_o the position of the wave maximum, is 1.4 cm and E_{or}, the zero order radial electric field, is -0.125 v/cm. Quantitative comparison between experiment and theory is made by solving Eq. (7) numerically for ω_R as a function of B with r_o = 1.4 cm, T = 2200°K, $n_o = 6.7 \times 10^{10}$ cm^{-3}, n_o'/n_o (n_o' is the density gradient at r_o) = -0.8 cm^{-1}, and $k_z = \pi/1.8L$ where L = 60 cm. k_z is determined from Eq. (13). From Figure 7 we observe two principal areas of agreement between the theory and exper-

ment. (1) The functional dependence of ω_R on B agrees with the predicted results. (2) The magnitude of the theoretical and experimental values agree within 25% in most cases. This is within the errors accumulated in measuring E_{or} and n_o'/n_o. In connection with this the value of E_{or} chosen for the calculation of the Doppler frequency, -0.125 v/cm, is the average of the measured values of E_{or} determined from the floating potential profiles. The same criteria is applied to n_o'/n_o where the value of $-0.8\ cm^{-1}$ is chosen from density profile measurements. As a further comment on the real frequency we also observe that its variation with magnetic field in the unstable regime is very similar to that for the externally driven modes just discussed. Because $e\phi_1/kT > 0.1$ and non-linear effects are present no attempt to compare the results to the linear theory is made. However it appears, qualitatively at least, that no significant changes in the behavior of ω_R vs. B take place between the linear, stable regime and this weakly non-linear ($0.1 < e\,\phi_1/kT < 0.2$) unstable case.

We next measure the linear growth rate as a function of B. After the excitation signal is shut off the received signal damps out as observed in Figure 3. The charactistic damping rate (ω_I) of such a signal is a combination of the end plate damping rate (ω_D) and the linear growth rate (ω_g). This can be expressed as

(22) $$\omega_g = \omega_D - \omega_I$$

Therefore by measuring ω_I from the scope traces and evaluating ω_D we can obtain the experimental values of ω_g. It is this quantity we are after since it is the expression determined by the dispersion relation, Eq. (7). The end plate damping rate is computed from Eq. (19) This computation, based on $n_o = 6.7\times10^{10} cm^{-3}$ and $T = 2200°K$, yields a

value of 1.4×10^{3} sec^{-1} for ω_D. As was discussed in section 2, ω_D is independent of magnetic field. Therefore changes in ω_i as B varies will be solely due to ω_g. Using this fact and substituting the value of ω_D into Eq. (22) we plot the experimental values of ω_g as a function of B for the m = 1, 2, and 3 modes in Figure 8. The theoretical curves are calculated from Eq. (7) based on the parameters given for the real frequency above. We observe the following areas of agreement. (1) The functional dependence of ω_g on B is that predicted. (2) The magnitude of the theoretical and experimental values agree within 25% for the m = 2 and m = 2 modes for most of the data. (3) The field at which $\omega_g = 0$ (cutoff field) for the m = 3 mode, B = 1750 gauss, is within 10% of the theoretically predicted value. Extrapolating the results for the m = 2 mode to $\omega_g = 0$ gives a value of B at cutoff (1200 gauss) which also agrees within 10%.

In connection with (1) we observe that ω_g increases with B for m = 2 (1200-1500 gauss) and m = 3 (1700-2100 gauss). In this regime viscous damping is important ($[k_\perp^2\rho_i^2 + t_{11}/t_\perp] > 0.3$) as discussed in section 2. These curves are well approximated by Eq. (12). For the other cases viscosity is no longer dominant and we observe ω_g decreasing as B increases. The variation of ω_g with B approaches that given by Eq.(10). With regard to (2) the errors in measuring k_z and use of the rectangular geometry approximation to the actual cylindrical geometry could account for the 25% discrepancy. Finally point (3) indicates clearly the mode dependence of the cutoff field demonstrated in section 2. The good agreement ($\sim$10%) between the experimental and theoretical values of the cutoff field obtained in this experiment results from (1) taking

end plate damping into account and (2) keeping the expressions $(1 + k_\perp^2\rho_i^2)$ and $(1 - k_\perp^2\rho_i^2)$ in the dispersion relation, Eq. (7). Previous measurements of the cutoff field were reported[3] which stated that the experimental values were about 50% higher than the theory predicted. However in this case neither of the two effects which we considered were taken into account in the computation of the cutoff field. As a final comment we note that the measured and computed values of ω_g for the m = 1 mode disagree by about a factor of two. We have no satisfactory explanation for this at this time. A possible source for this discrepancy is the fact that k_x, which is equal to k_y, is also approximately equal to n_o'/n_o. Therefore the localization approximation used to neglect k_x terms in the dispersion relation is not as valid as for the higher modes. In connection with this Chen[25] has shown for drift waves in cylindrical geometries excluding ion viscosity that the growth rate when radial dependence (hence x) is included is about three times as large as in the case when radial dependence is neglected.

D. Variation of the Plasma Column Length

Measurement of ω_R as a function of plasma column length is performed by using the bellows assembly as described in section 3. The results of this measurement are shown for an m = 3 mode in Figure 9. The value of ω_R is plotted after subtracting the Doppler frequency, Eq. (21), with a value of E_{or} = -0.20 v/cm and r_o = 1.8 cm. The frequency is observed to decrease with increasing L. This reflects the effect of ion viscosity which results in ω_R becoming a function of k_z as seen in Eq. (8) and described in section 2. The theoretical curve is calculated from Eq. (7). We observe the following areas of agree-

ment. (1) The functional variation of ω_R on L is that predicted. (2) The magnitude of the theoretical and experimental values of ω_R agree within 25%.

We next perform a measurement of ω_g as a function of L. The procedure is to measure ω_I and then determine ω_D from Eq. (19) in order to calculate ω_g from Eq. (22). In this case, however, since ω_D is a function of L we must determine ω_D at every value of L. The results of such a measurement are displayed in Figure 9 for an m = 3 mode. We observe that ω_g is relatively independent of L. This is a consequence of the viscous contribution to ω_g discussed in section 2 and expressed in Eq. (12). The net result is that the change in the measured net damping rate (ω_I) is due almost entirely to changes in ω_D. The theoretical curve plotted in Figure 9 is calculated form Eq. (7). We obtain the following areas of agreement. (1) The theoretical and experimental values agree within 25%. (2) The relative independence of ω_g as a function of L is confirmed. (3) The dependence of end plate damping on L is demonstrated since the observed change in ω_D (end plate damping rate) over the range of L tested is within 15% of that calculated.

E. Phase Angle Measurement

As discussed in section 2 the phase angle (θ) between the density perturbation and the potential perturbation is an important parameter since it determines the growth rate of the drift wave in the non-viscous regime ($[b + t_{\parallel}/t_{\perp}] < 0.3$). This angle is measured as a function of magnetic field and compared to the corresponding growth rate. Previous measurements have been made of this angle for drift waves in the unstable regime.[3] However they have been made at only a single

value of B and no correlation with the growth rate has been presented. The results of our measurements for an m = 2 mode in the regime where viscosity is not dominant are displayed in Figure 10. In this case the growth rate is dependent principally on the phase angle as discussed in section 2. In making the measurements of the density perturbation in order to determine the phase angle we must consider that the biased probe is collecting the entire perturbed flux which is

$$J_i = n_i e v_{ith} + n_o e v_i$$

where v_i is the perturbed ion velocity and v_{ith} is the ion thermal velocity. Therefore the phase angle we measure is between J_i/J_o, where $J_o \sim n_o e v_{ith}$, and $e\phi_i/kT$. The expression derived in Eq. (14) accounts for only the first term in J_i. A relation can be derived between J_i/J_o and $e\phi_i/kT$ by calculating v_i from the perturbed ion velocities obtained from the first order equations of motion and n_i/n_o from the continuity equations. From this the phase angle is easily obtained and is given by

$$(14)' \qquad \tan\theta = - \frac{b(\omega_R + k_y v_D) t_{ii}}{1 + t_{ii}(b)^{3/2}(\omega_R + k_y v_D)} .$$

This is the angle actually measured in the experiment. However for our experimental conditions the term $t_{ii}(b)^{3/2}(\omega_R + k_y v_D)$ is ≤ 0.1 and Eq. (14)' is very nearly the same as Eq. (14). It is apparent, though, that under conditions of large t_{ii} and/or large $k_\perp \rho_i$ the contribution from the $n_o e v_i$ term to the measured phase angle is significant and must be included in the analysis. From Figure 10 we see that the density perturbation (n_i) leads the potential perturbation (ϕ_i) and that the growth rate decreases as the phase angle decreases as we vary the

magnetic field. The results are compared with the theoretical expression for tanΘ from Eq. (14). The experimental values of ω_R are used in the calculation. We observe that the functional dependence of Θ on B is that predicted and that the experimental and theoretical values agree within 25% for most of the data points.

Observations of the phase angle as a function of B in the viscous dominated range ($[b + t_{11}/t_{\perp}] > 0.3$) show two different types of behavior. For low densities, ($<5\times10^{10}$ cm^{-3}), we observe that both Θ and ω_g increase in magnitude with increasing B as displayed in Figure 11. For densities $> 5\times10^{10}$ cm^{-3}, no change in Θ is detectable as we vary B even though ω_g increases with B. In the first case the observed behavior is not the predicted by the theory and the physical picture presented in section 2. The reason for the discrepancy is not understood at this time. In the second case, that of densities greater than 5×10^{10} cm^{-3}, the results agree qualitatively with those predicted in that we expect the increasing ion inertia contribution to tanΘ to nearly balance the decreasing FLR portion resulting in a slowly decreasing phase angle.

V. CONCLUSIONS

In this work we have presented a study of the linear characteristics of drift waves. We find that the method of external excitation of drift waves by a grid provides a powerful tool in examining the linear behavior of drift waves just as in the case of ion acoustic waves.[15] In this manner we are able to limit our selves to small amplitude ($e\phi_1/kT < 0.1$) oscillations in order to investigate the linear theory of these waves.

Our work has demonstrated the following:

1) The axial wavelength of drift waves is found to depend on the sheath conditions at the cathodes and on the length of plasma column.

2) End plate damping has a signigicant influence on the stability of drift waves in a bounded system. When the sheaths at the cathode are ion rich the recombination loss of the perturbation at the cathodes is sufficient to damp out the drift wave. The damping rate is reduced considerably when electron sheaths are present.

3) The behavior of the real and imaginary frequencies of the drift wave as a function of the magnetic field and plasma column length is shown to obey the linear dispersion relation including ion viscosity and finite Larmor radius and when the effects of end plate damping are considered.

4) The predicted functional dependence of the phase angle is confirmed. In addition correlation between the growth rate and the magnitude of the phase angle is demonstrated when ion viscosity does not dominate the behavior of the drift wave.

ACKNOWLEDGMENTS

We are grateful to Dr. Francis Hal for his able assistance in performing the experiment and for many valuable discussions of the problem. We wish to acknowledge the capable help of Mr. Zalton Lucky and the UCLA Plasma Physics Group.

This paper is based on a thesis submitted by one of us (R.E.R.) in Dec. 1968 to UCLA in partial fulfillment of the requirements for the Ph.D. degree. This work was supported by funds from NASA Grant No. NGR05-007-066.

REFERENCES

1. T.H. Stix, Phys. Rev. Letters 20, 1422 (1968).

2. T. H. Dupree, Unpublished report.

3. H. W. Hendel, T. K. Chu, and P. A. Politzer, Phys. Fluids 11, 2426 (1968).

4. B. J. Eastland, K. Josephy, R. F. Leheny, and T. C. Marshall, Phys. Fluids 9, 2400 (1966).

5. L. I. Rudakov and R. Z. Sagdeev, Sov. Phys. Dokl. 6, 415 (1961).

6. B. B. Kadomtsev and A. K. Timofeev, Sov. Phys. Dokl. 7, 826 (1963).

7. M. N. Rosenbluth and N. A. Krall, Phys. Fluids 6, 254 (1963).

8. M. N. Rosenbluth, Plasma Physics, (International Atomic Energy Agency, Vienna, 1965) p. 485.

9. A. A. Galeev, S. S. Moiseev, and R. Z. Sagdeev, J. Nucl. Energy, Pt. C 6, 645 (1964).

10. F. F. Chen, Phys. Fluids 8, 912 (1965); Phys. Fluids 8, 1323 (1965).

11. B. Coppi, H. W. Hendel, F. Perkins, and P. A. Politzer, Proceedings of Conference on Physics on Quiescent Plasmas (Laboratori Gas Ionizzati, Frascati, Italy, 1967) Part 1, p. 201.

12. N. D'Angelo and R. W. Motley, Phys. Fluids 6, 422 (1963).

13. H. Lashinsky, Phys. Rev. Letters 12, 121 (1964).

14. N. S. Buchelnokova, Sov. Physics JETP 19, 775 (1964).

15. A. Y. Wong, R. W. Motley, and N. D'Angelo, Phys. Rev. 133, A436 (1964).

16. F. Hai and A. Y. Wong, University of California, Los Angeles, Plasma Physics Group Report No. 40 , Feb. 1969 (unpublished).

17. D. C. Montgomery and D. A. Tidman, Plasma Kinectic Theory, (McGraw-Hill Book Co. New York, 1964) p. 205.

18. F. F. Chen, J. Nucl. Energy, Pt. C 7, 399 (1965).

19. F. F. Chen, Private Communication.

20. J. J. Wada, Hughes Research Laboratiies Report No. 306 (1963) p. 236.

21. N. Rynn and N. D'Angelo, Rev. Sci. Instr. 31, 1326 (1960).

22. A. Y. Wong and R. Rowberg, Phys. Rev. Letters 18, 390 (1967).

23. F. F. Chen, Princeton Plasma Physics Laboratory Report MATT-520 1967 (unpublished).

24. S. vonGoeler, Phys, Fluids 7, 463 (1964).

25. F. F. Chen, Phys. Fluids 10, 1647 (1967).

FIGURE CAPTIONS

1. Schematic of the rectangular geometry for the drift wave. We have displayed the zero order quantities and the perpendicular (y) perturbation. Also shown is a schematic of the drift wave in the cylindrical geometry giving the axial (z) perturbetion and showing the perpendicular and axial propagation.

2. Radial amplitude profiles showing the separation of the density gradient drift wave (1) and the edge oscillation (2) relative to the density and floating potential profiles and the tungsten ionizer plate (5.8 cm in diameter). The vertical scale is arbitrary. The peak density is 1×10^{11} cm^{-3} and n_1/n_o for the drift wave is < 0.07. E_{or} (the slope of potential profile at r_o) is -0.15 v/cm where r_o = 1.3 cm. Potassium plasma, T = 2200°K.

3. Schematic of the experimental set-up. The excitation signal can be fed in steady state or gated through the tone burst generator. The signals can be received through either the ion saturation bias network or the high frequency circuit for floating potential flucuations.

4. The upper trace is the gated excitation signal. The vertical scale is 2v/cm for this trace. The lower trace is the received signal ahowing the characterisiic damping when the gate of the tone burst generator is closed. The vertical scale for this trace is 1v/cm. The value of n_1/n_o < 0.07. The horizontal scale is 1.0 msec/cm.

5. Wave amplitude as a function of axial distance for double ended operation of the Q-device. The upper curve is for ion rich sheaths

giving an axial wavelength of about 4L. The lower curve is for electron rich sheaths giving an axial wavelength of 2L. The solid lines are the theoretical curves proportional to $\cos(k_z z)$ where k_z is determined from Eq. (13).

6. Wave amplitude profiles as a function of axial distance for two values of L. Sheaths are electron rich so that the axial wavelength is approximately 2L. The measurements extend from the column center to a value of z close to one of the plates. The upper curve is for a column length of 60 cm and the bottom curve for L = 46 cm. The solid lines are the theoretical curves which are proportional to $\cos(k_z z)$. k_z is determined from Eq. (13).

7. Real frequency of the externally excited drift wave as a function of magnetic field for the m = 1, 2, and 3 modes. $e\phi_1/kT < 0.05$. The Doppler frequency due to the zero order electric field has been subtracted from the measured frequencies. $E_{or} = -0.125$ v/cm at $r_o = 1.4$ cm for this case. The solid lines are the theoretical curves calculated from Eq. (7). Potassium plasma, T = 2200°K.

8. Growth rate of the externally excited drift wave as a function of the magnetic field for the m = 1, 2, and 3 modes. $e\phi_1/kT < 0.05$. The growth rates (ω_g) plotted are obtained from the measured damping (ω_I) by taking into account the end plate damping (ω_D), calculated from Eq. (19), according to the relation $\omega_g = \omega_D - \omega_I$. The solid lines are the theoretical curves calculated from Eq. (7). Potassium plasma, T = 2200°K.

9. Real frequency (a) and growth rate (b) of the externally excited drift wave as a function of column length for the m = 3 mode. $e\phi_1/kT < 0.05$. (a) The Doppler frequency has been subtracted out from the measured frequencies. In this case $E_{or} = -0.2$ v/cm at $r_o = 1.8$ cm. (b) The measured damping has been adjusted for end plate damping before being plotted. ω_D is calculated from Eq. (19) for each value of L in this case. The solid lines are the theoretical curves calculated from Eq. (7). Potassium plasma, T = 2200°K.

10. Density-potential flucuation phase angle and growth rate for the externally excited drift wave as a function of magnetic field. A negative phase angle means that n_1 leads ϕ_1. $e\phi_1/kT < 0.05$. The curves are for an m = 2 mode. Because $[b + t_{11}/t_{\perp}] < 0.3$ we are in the regime where ion viscosity is no longer dominant and the curves show the correlation between the growth rate and the phase angle as a function of field. The solid lines are the theoretical curves. For the growth rate they are calculated from Eq. (7). For the phase angle they are calculated from Eq. (14). Potassium plasma, T = 2200°K.

11. Density-potential flucuation phase angle and growth rate for the externally excited drift wave as a function of magnetic field. A negative phase angle means that n_1 leads ϕ_1. $e\phi_1/kT < 0.05$. Since $[b + t_{11}/t_{\perp}] > 0.4$ we are within the viscous dominated regime as indicated by the behavior of ω_g. The correlation between ω_g and the phase angle is not predicted by the theory (Eq. (14)) and remains unresolved at this time. Potassium plasma, T = 2200°K.

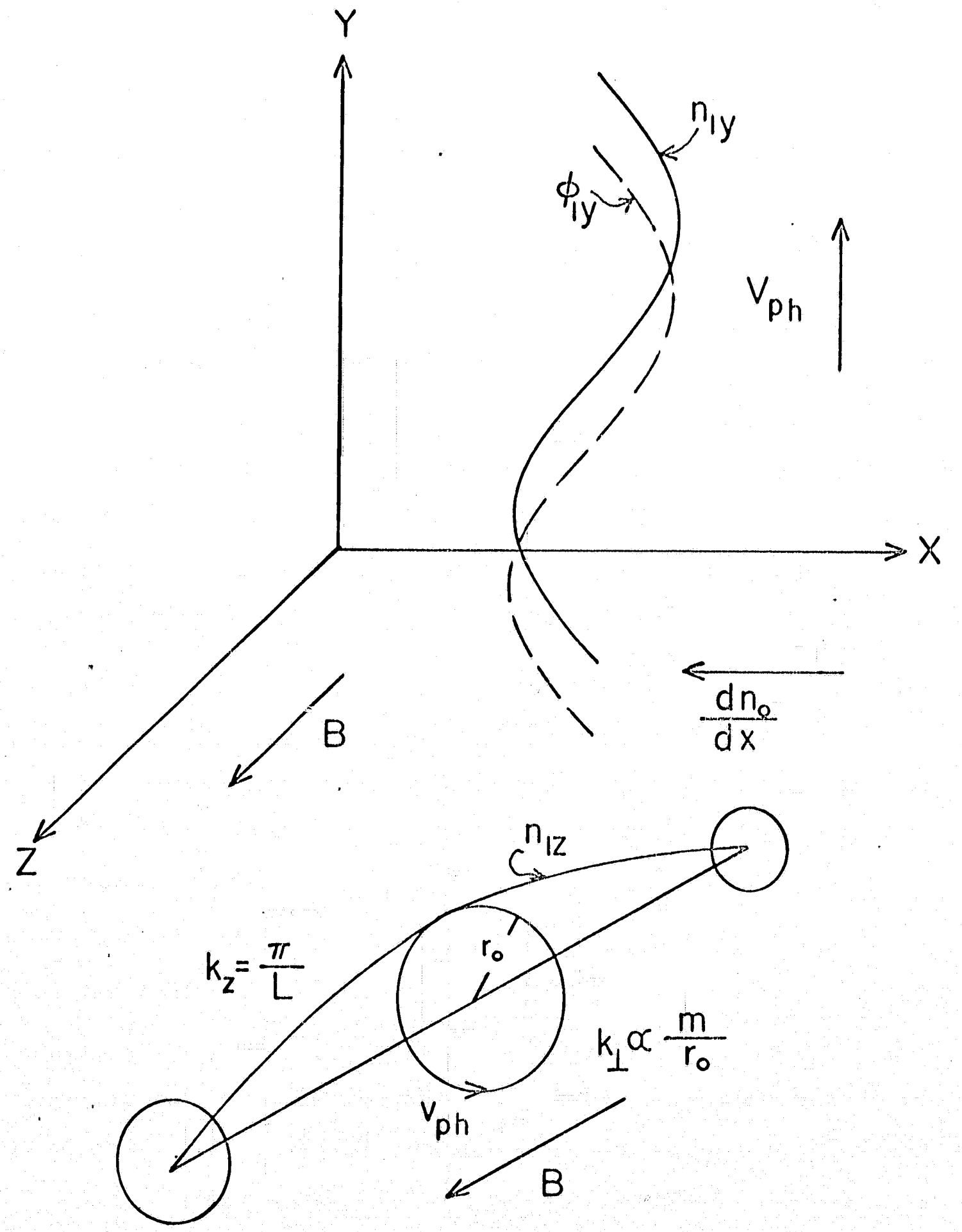
Y
X
Z
B
n_{1y}
ϕ_{1y}
V_{ph}
$\frac{dn_o}{dx}$
n_{1z}
$k_z = \frac{\pi}{L}$
r_o
$k_\perp \propto \frac{m}{r_o}$
V_{ph}
B

FIGURE 1

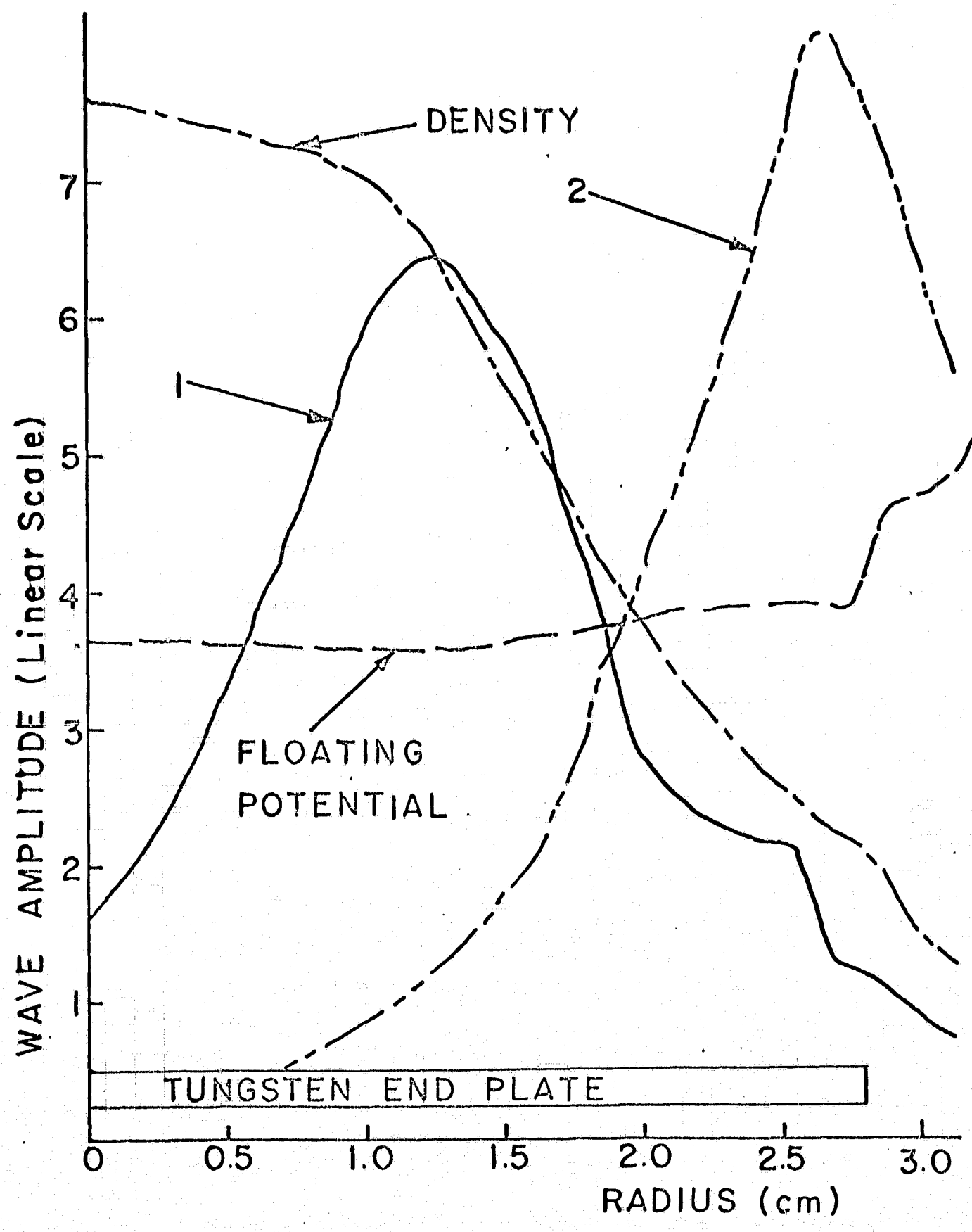
DENSITY
2
1
FLOATING
POTENTIAL
TUNGSTEN END PLATE
WAVE AMPLITUDE (Linear Scale)
7
6
5
4
3
2
1
0
0.5
1.0
1.5
2.0
2.5
3.0
RADIUS (cm)

FIGURE 2

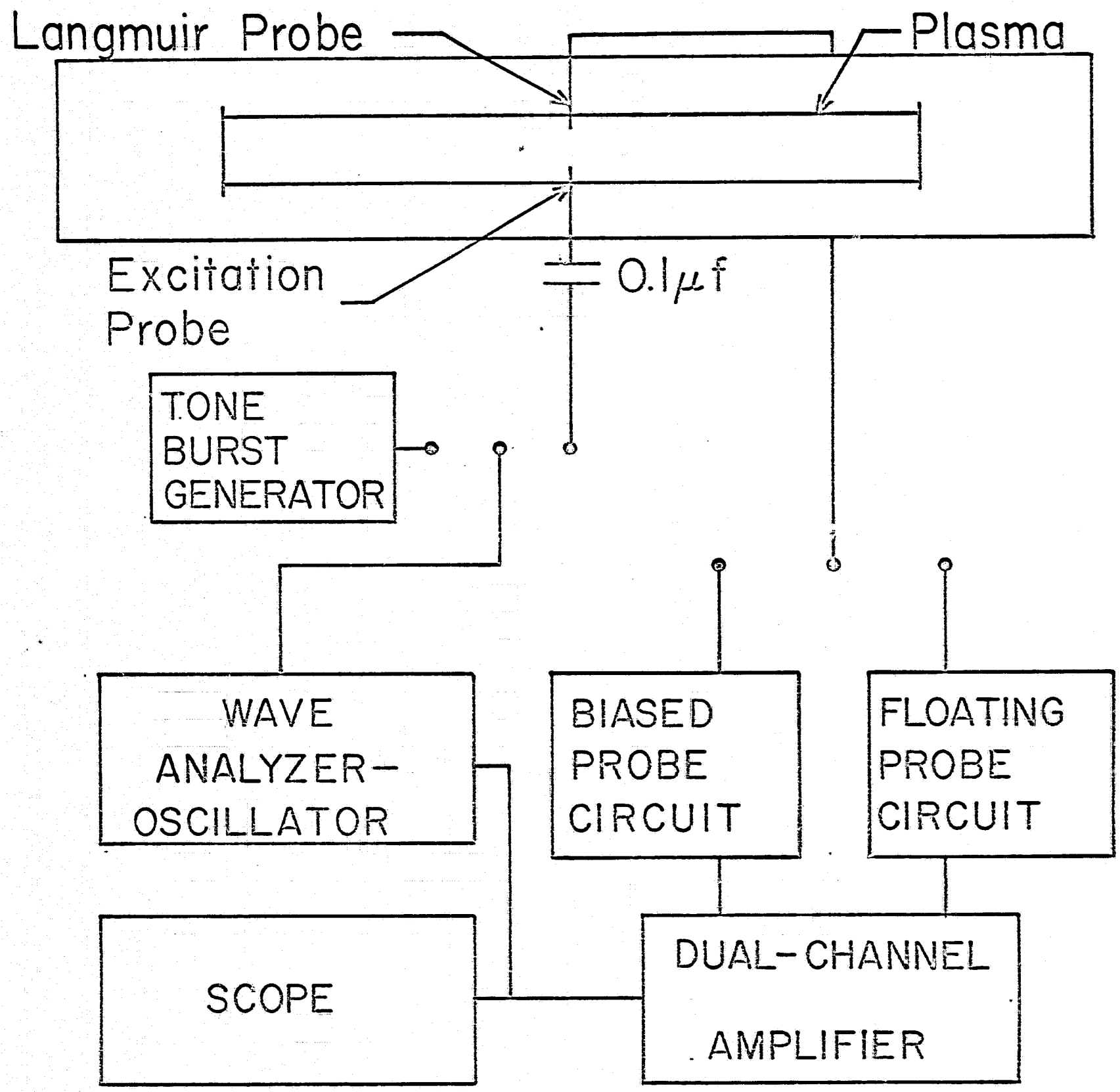
Langmuir Probe
Plasma
Excitation Probe
0.1μf
TONE BURST GENERATOR
WAVE ANALYZER-OSCILLATOR
BIASED PROBE CIRCUIT
FLOATING PROBE CIRCUIT
SCOPE
DUAL-CHANNEL AMPLIFIER

FIGURE 3

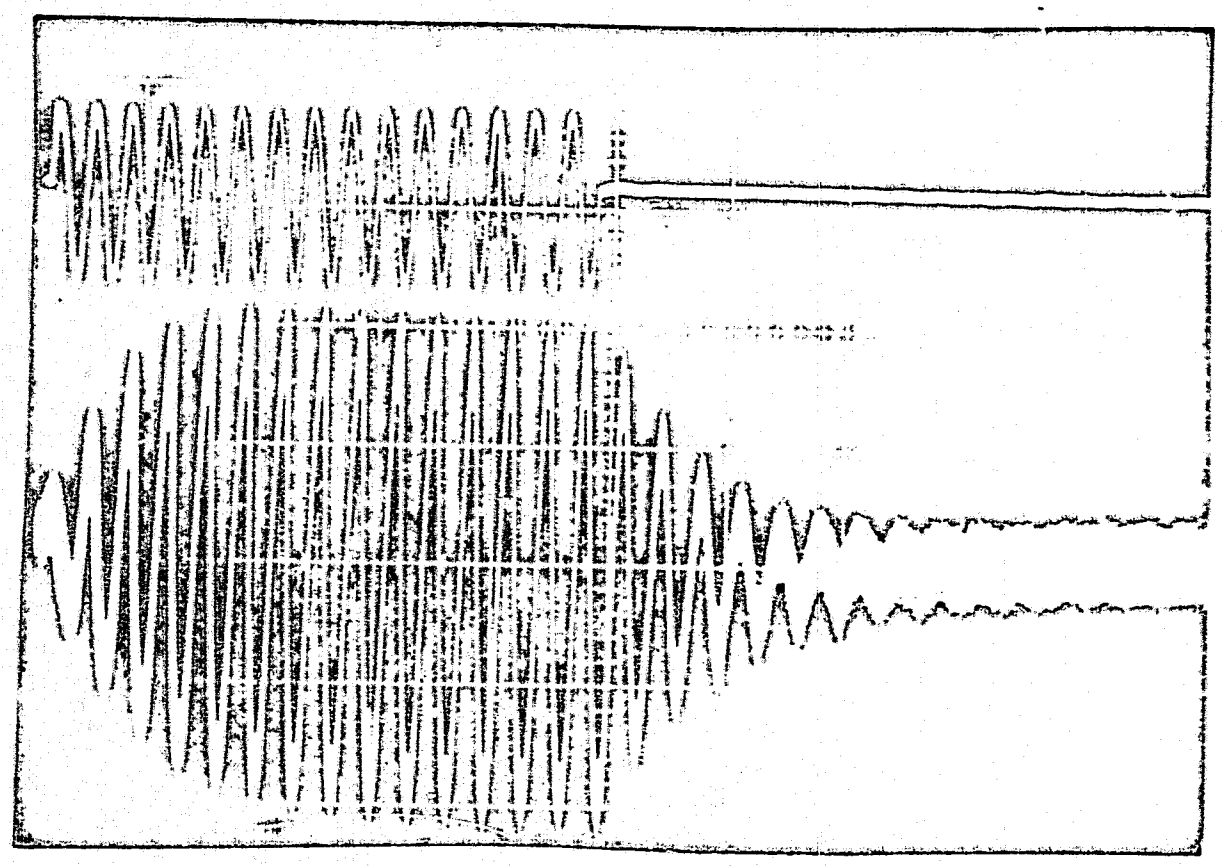

EXCITATION SIGNAL
SCALE – 2v/cm

PLASMA RESPONSE
SCALE – 0.1mv/cm

HORIZONTAL SCALE – 1.0 ms/cm

FIGURE 4

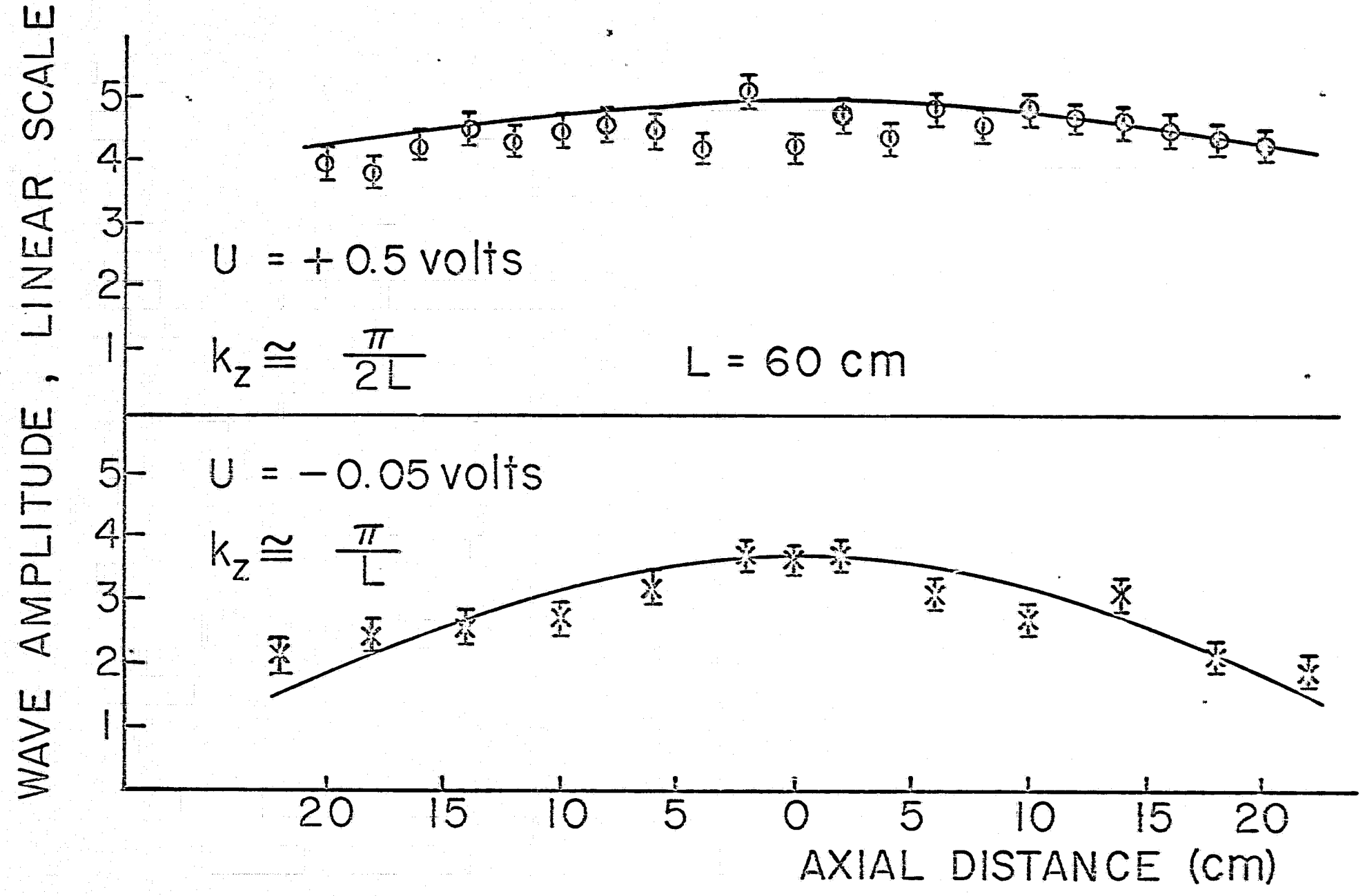
WAVE AMPLITUDE, LINEAR SCALE
1
2
3
4
5
U = +0.5 volts
$k_z \cong \frac{\pi}{2L}$
L = 60 cm
U = −0.05 volts
$k_z \cong \frac{\pi}{L}$
20
15
10
5
0
5
10
15
20
AXIAL DISTANCE (cm)

FIGURE 5

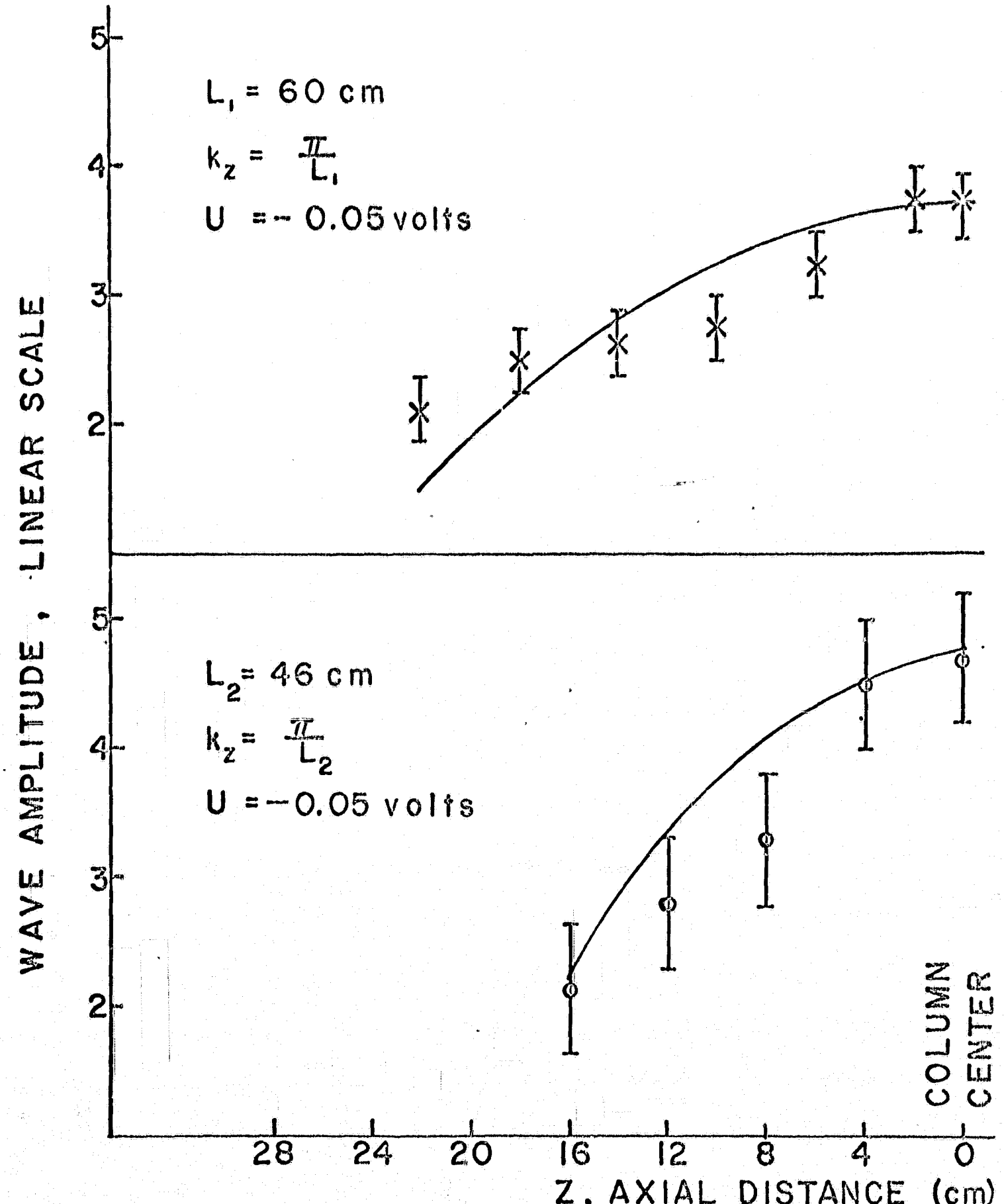
WAVE AMPLITUDE, LINEAR SCALE
5
4
3
2
L_1 = 60 cm
$k_z = \frac{\pi}{L_1}$
U = − 0.05 volts
L_2 = 46 cm
$k_z = \frac{\pi}{L_2}$
U = −0.05 volts
COLUMN CENTER
28
24
20
16
12
8
4
0
Z, AXIAL DISTANCE (cm)

FIGURE 6

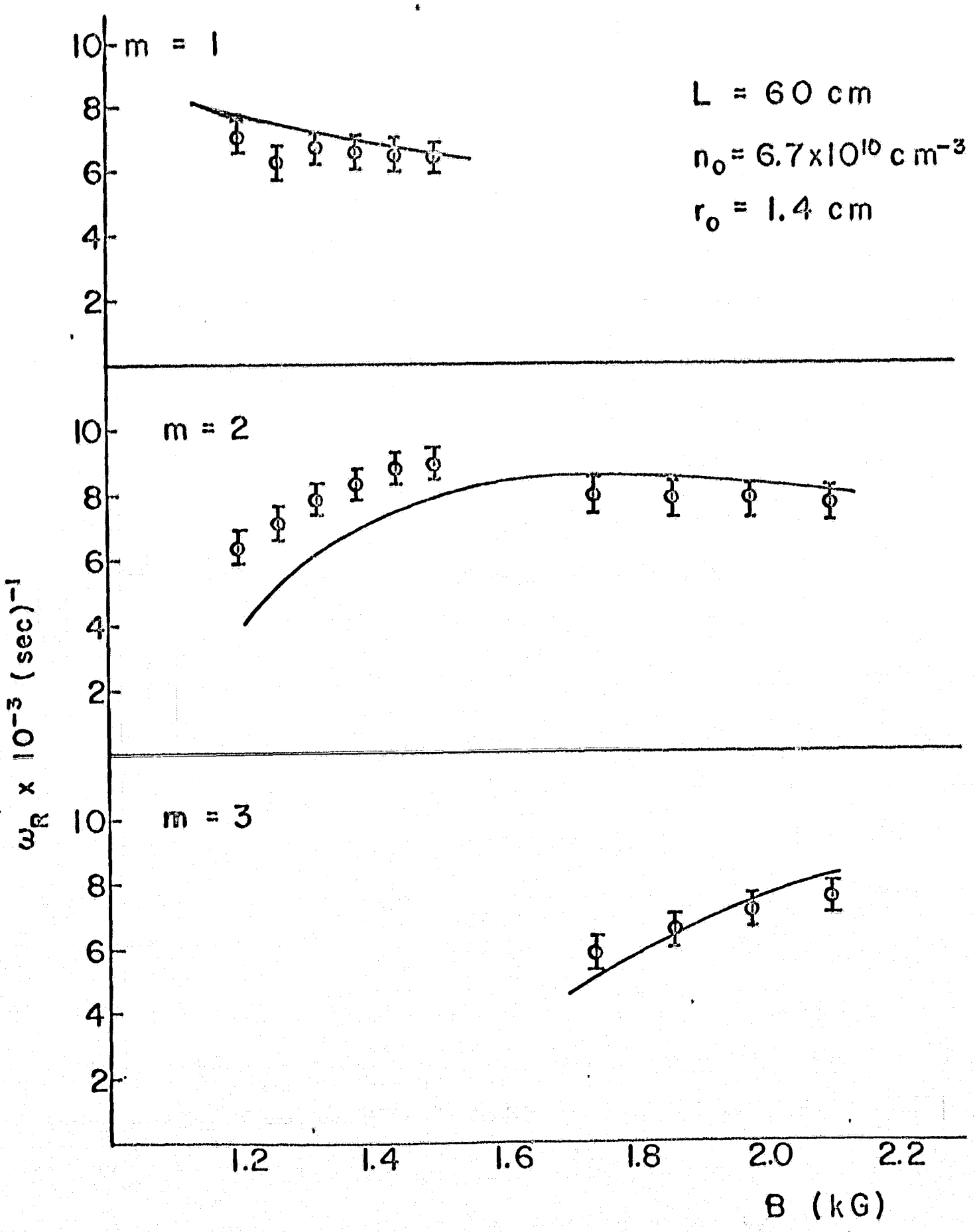
m = 1
m = 2
m = 3
L = 60 cm
$n_o = 6.7 \times 10^{10}$ cm^{-3}
r_o = 1.4 cm
$\omega_R \times 10^{-3}$ (sec)$^{-1}$
10
8
6
4
2
1.2
1.4
1.6
1.8
2.0
2.2
B (kG)

FIGURE 7

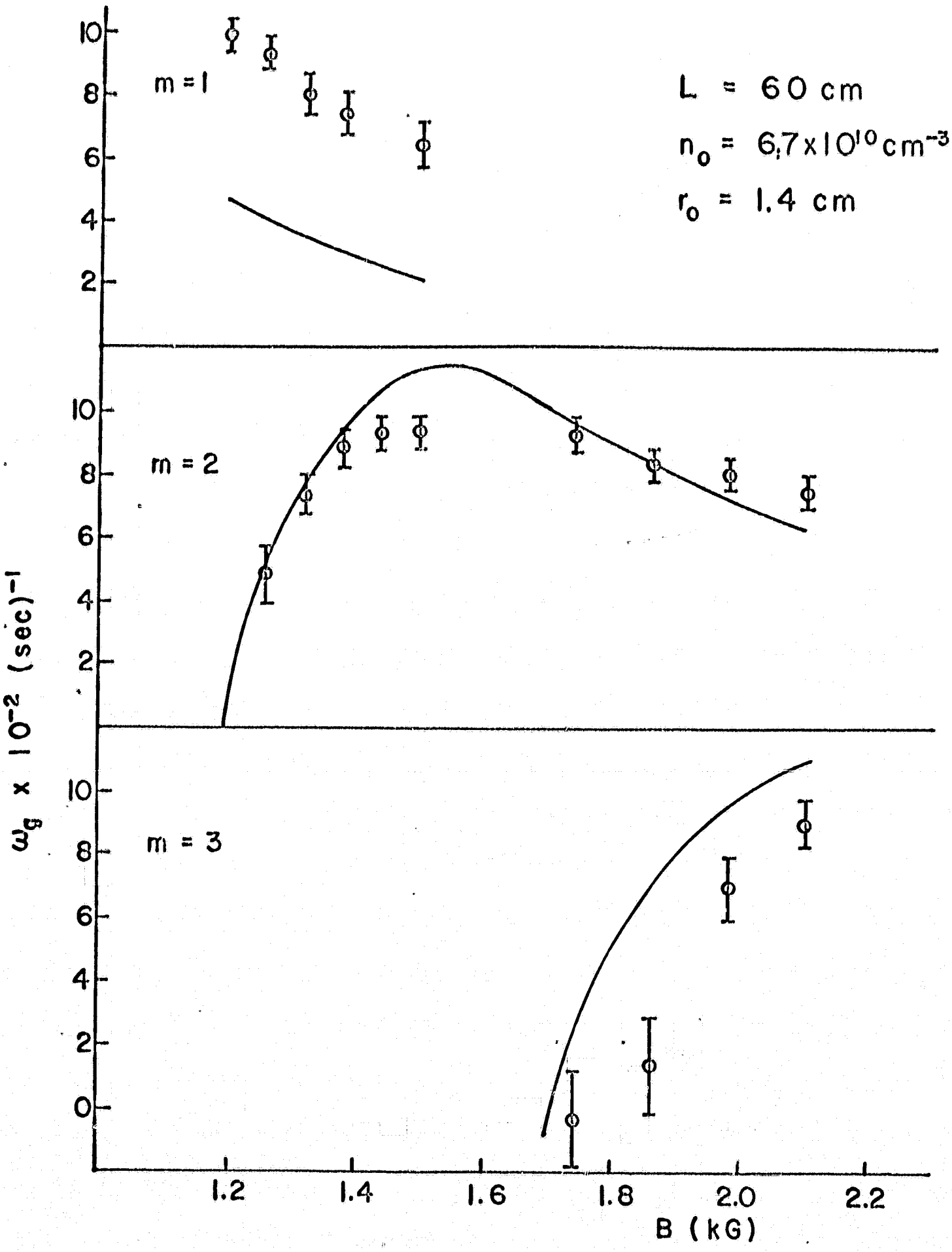
m = 1
m = 2
m = 3
L = 60 cm
n_o = 6.7x10^{10} cm^{-3}
r_o = 1.4 cm
ω_g x 10^{-2} (sec)$^{-1}$
B (kG)
10
8
6
4
2
0
1.2
1.4
1.6
1.8
2.0
2.2

FIGURE 8

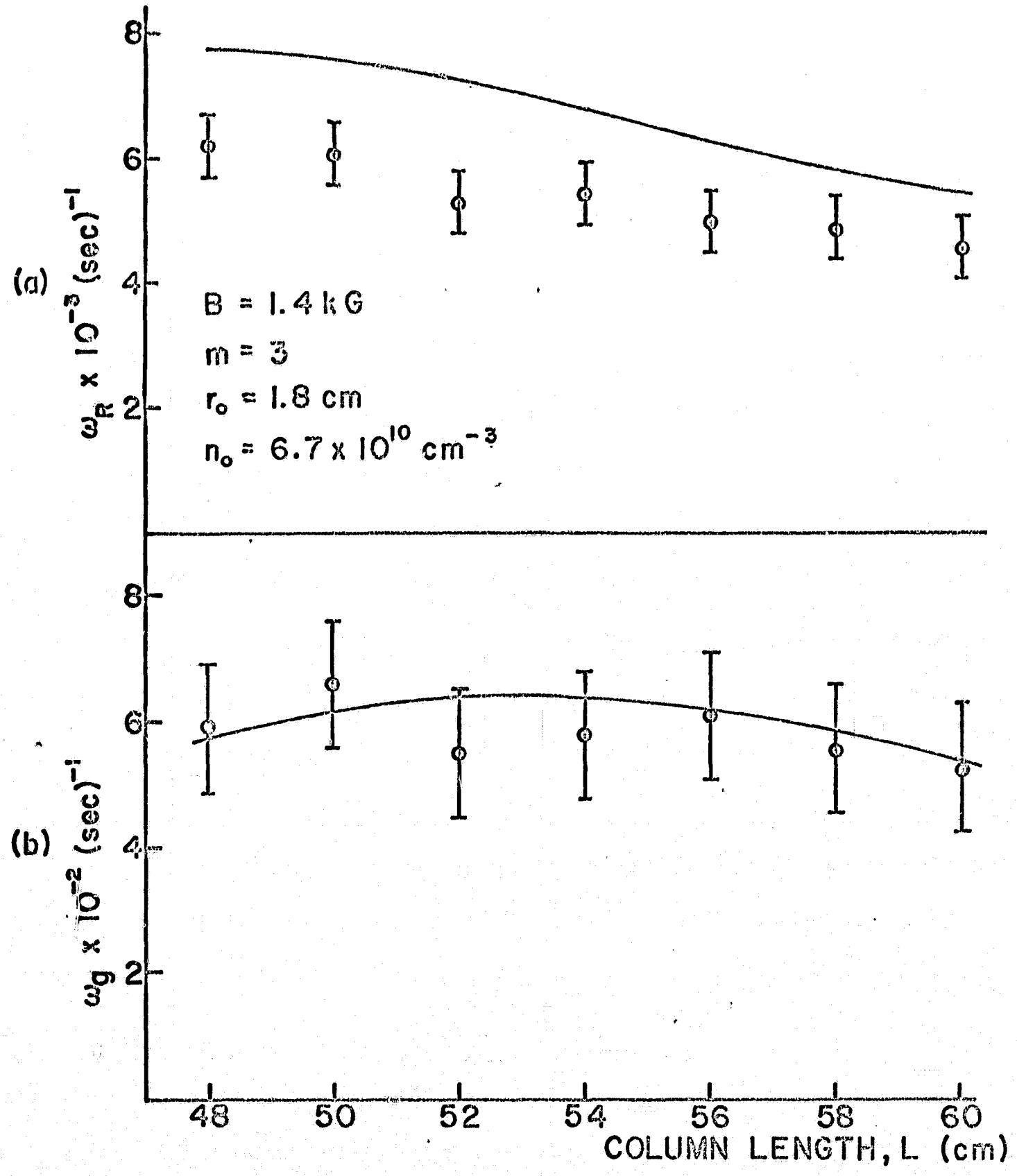
(a)
$\omega_R \times 10^{-3}$ (sec)$^{-1}$
8
6
4
2
B = 1.4 kG
m = 3
r_o = 1.8 cm
n_o = 6.7×10^{10} cm^{-3}
(b)
$\omega_g \times 10^{-2}$ (sec)$^{-1}$
8
6
4
2
48
50
52
54
56
58
60
COLUMN LENGTH, L (cm)

FIGURE 9

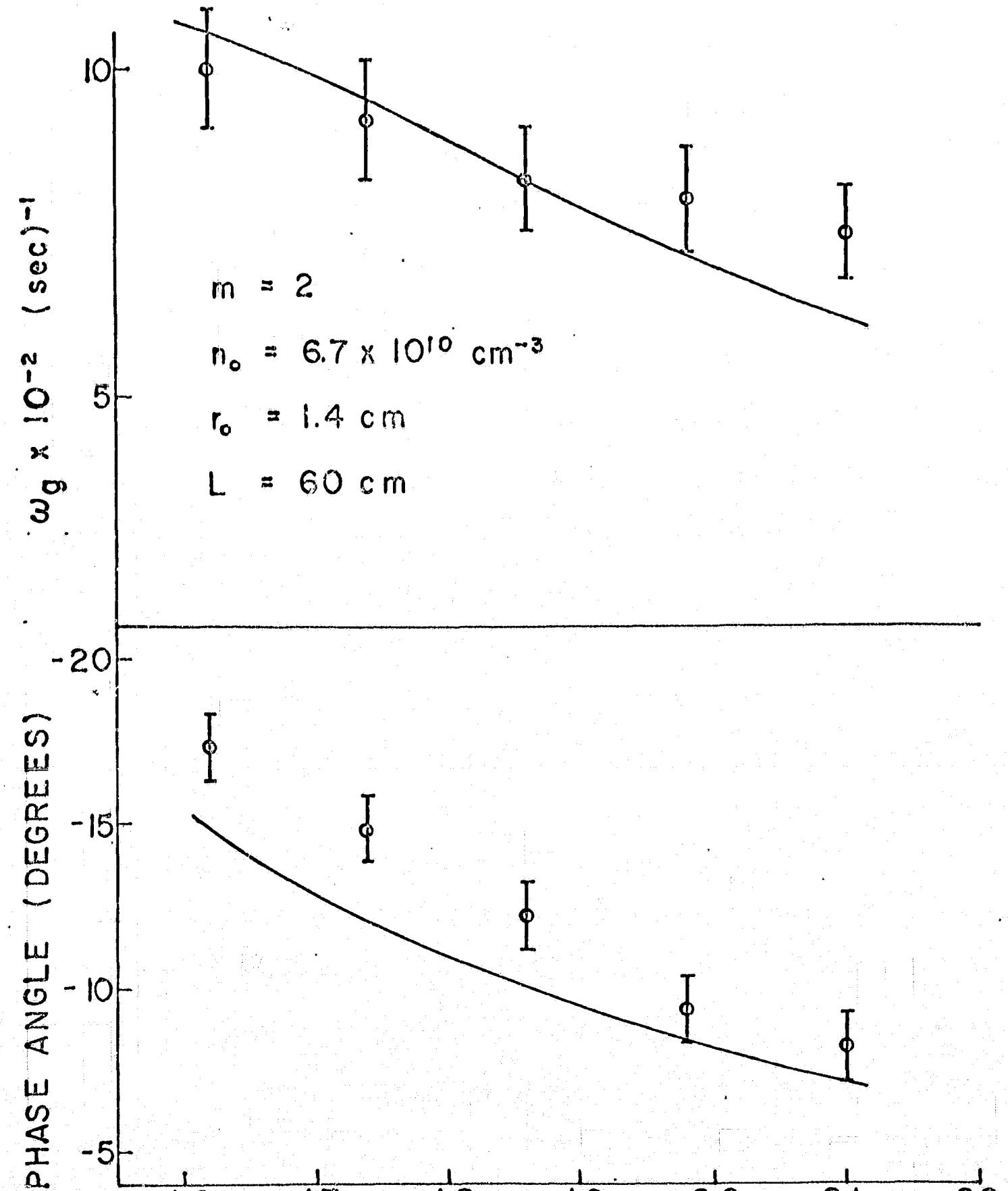
10
5
$\omega_g \times 10^{-2}$ (sec)$^{-1}$
m = 2
n_o = 6.7 x 10^{10} cm^{-3}
r_o = 1.4 cm
L = 60 cm
-20
-15
-10
-5
PHASE ANGLE (DEGREES)
1.6
1.7
1.8
1.9
2.0
2.1
2.2
MAGNETIC FIELD (kG)

FIGURE 10

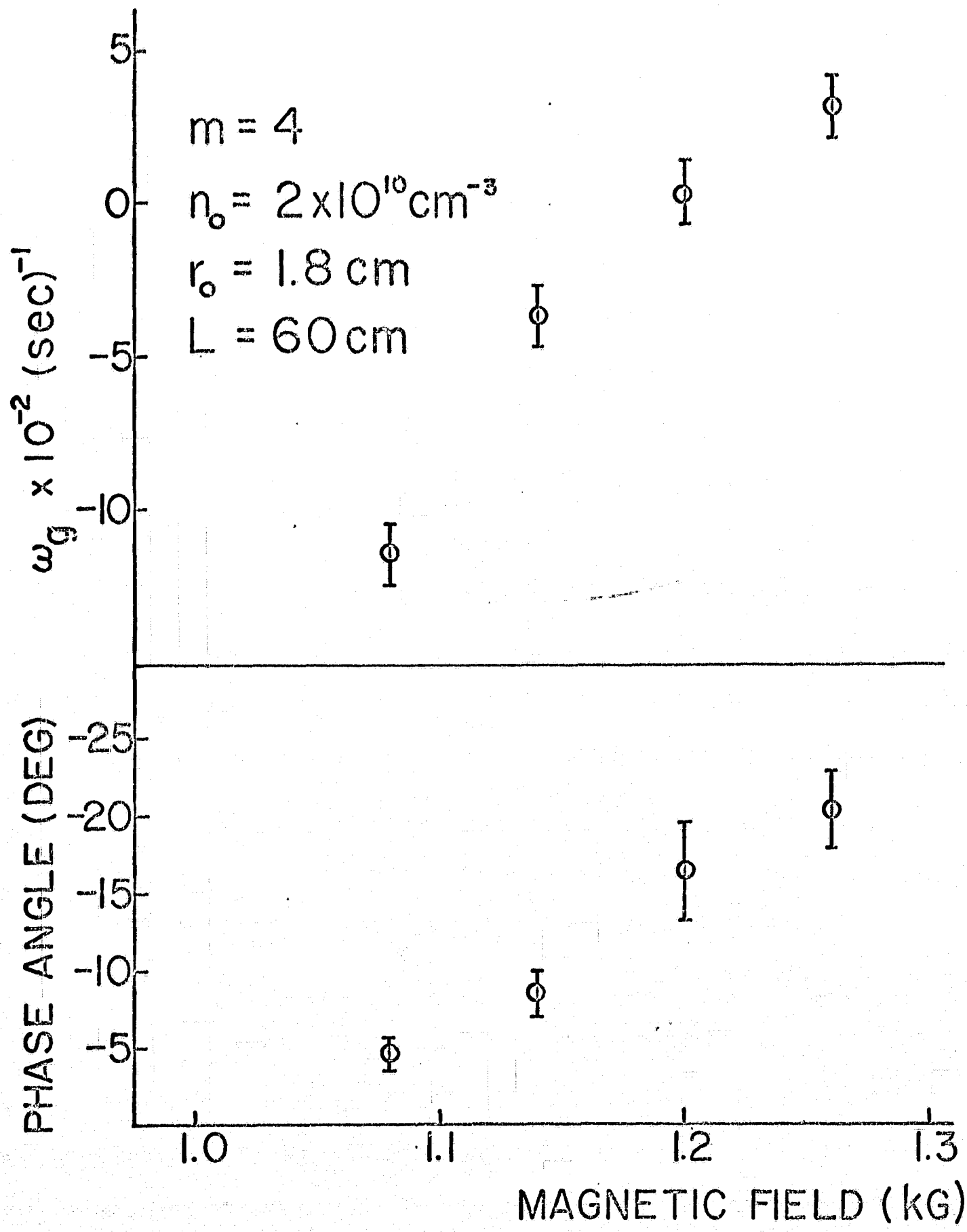
m = 4
$n_o = 2 \times 10^{10} cm^{-3}$
$r_o = 1.8$ cm
L = 60 cm
$\omega_g \times 10^{-2}$ (sec)$^{-1}$
5
0
-5
-10
PHASE ANGLE (DEG)
-25
-20
-15
-10
-5
1.0
1.1
1.2
1.3
MAGNETIC FIELD (kG)

FIGURE 11

APPENDIX

In this appendix we present the details of the calculation of the of the dispersion relation (Eq. 7). The assumptions used are those listed in the text. In this section we solve the equations of motion for the ions inzero and first order and obtain the first order ion continuity equation. The same procedure is followed for the electrons. With the assumption of quasi-neutrality the continuity equations for the two species are combined to yield the dispersion relation relating ω and $\underline{k}$. This equation is then solved for several limiting cases.

Since only ion motion perpendicular to $\underline{B}$ occurs we can write down the equation of motion for ions as

$$(1)\quad nM\left(\frac{\partial \underline{V}_\perp}{\partial t} + \underline{V}_\perp \cdot \nabla_\perp \underline{V}_\perp\right) = ne\left[\underline{E}_\perp + \frac{\underline{V}_\perp \times \underline{B}}{c}\right] - \nabla_\perp p - \nabla_\perp : \underline{\underline{\pi}} + \underline{F}_g n_o = 0$$

p is the scalar pressure equal to nkT, $\underline{\underline{\pi}}$ is the pressure tensor and is a first order quantity, and $\underline{F}_g$ is a generalized gravitational force. The latter is usually the representation in rectangular geometry of the centrifugal force arising from an $\underline{E}\times\underline{B}$ rotation of a cylindrical plasma due to a zero order radial electric field. The effects of this force on the growth rate and real frequency are small compared to the remaining terms for our experimental conditions so this force is neglected. As a consequence the only effect a zero order electric field has is to add a Doppler shift to the real frequency. The Doppler frequency is subtracted from the data and therefore we can solve the equations in a reference frame moving with the $\underline{E}\times\underline{B}$ drift of the zero order electric field. The

zero order steady state equation then becomes with $\underline{v}_\perp = \underline{v}_{o\perp}$,

$$0 = n e\left[\frac{\underline{V}_{o\perp} \times \underline{B}}{c}\right] - \nabla(n_o KT) = 0 \tag{2}$$

Since $\nabla_\perp n_o = dn_o/dx\,\hat{x}$ and $\underline{B} = B\hat{z}$, the only component we have of (2) is the x component. Therefore we solve for $\underline{V}_{o\perp}$ to get

$$V_{oy} = c\frac{KT}{eB}\frac{n_o'}{n_o} \equiv -V_D \tag{3}$$

where v_D is the electron diamagnetic drift velocity.

The first order motion is obtained by linearizing Eq. (1) with $\underline{v}_\perp = \underline{v}_1 + \underline{v}_o$, $n = n_1 + n_o$, and $\underline{E}_\perp = -\nabla_\perp\phi$. Therefore Eq. (1) becomes

$$\left(\frac{\partial \underline{V}}{\partial t} + \underline{V}_1\cdot\nabla_\perp\underline{V}_o + \underline{V}_o\cdot\nabla_\perp\underline{V}_1\right) = \frac{e}{M}\left[-\nabla_\perp\phi_1 + \frac{\underline{V}_1\times\underline{B}}{c}\right] + \frac{n_1}{n_o}\frac{KT}{M}\nabla_\perp n_o -$$
$$-\frac{1}{n_o}\frac{KT}{M}\nabla_\perp n_1 - \frac{1}{n_o M}\nabla_\perp\cdot\underline{\underline{\Pi}} \tag{4}$$

after dividing by $n_o M$. This is simplified by using

$$\frac{KT}{M}\left(\frac{n_1}{n_o}\nabla_\perp n_o - \frac{\nabla_\perp n_1}{n_o}\right) = -\frac{KT}{M}\nabla_\perp\left(\frac{n_1}{n_o}\right). \tag{5}$$

The terms $\underline{v}_1\cdot\nabla_\perp\underline{V}_o + \underline{V}_o\cdot\nabla_\perp\underline{v}_1$ can be written using Eq. (3) and the assumption $\partial/\partial x\,(n_o'/n_o) = 0$ as

$$V_{oy}\left(\frac{\partial V_x}{\partial x}\hat{x} + \frac{\partial V}{\partial y}_y\hat{y}\right) \tag{6}$$

Finally the expression for $\underline{\underline{\Pi}}$ is written to first order as

$$\underline{\underline{\Pi}} = -\frac{\alpha_1 n_o KT}{2\omega_c}\begin{pmatrix} \frac{\partial V_x}{\partial x} + \frac{\partial V_x}{\partial y} & \frac{\partial V_y}{\partial y} - \frac{\partial V_x}{\partial x} \\ \frac{\partial V_x}{\partial y} - \frac{\partial V_y}{\partial x} & -\frac{\partial V_y}{\partial x} - \frac{\partial V_x}{\partial y} \end{pmatrix} - \tag{7}$$

$$- \frac{\alpha_2 n_0 KT}{5\omega_c} \nu_{ii} \begin{pmatrix} \frac{\partial v_x}{\partial x} - \frac{\partial v_y}{\partial y} & \frac{\partial v_y}{\partial x} + \frac{\partial v_x}{\partial y} \\ \frac{\partial v_y}{\partial x} + \frac{\partial v_x}{\partial y} & \frac{\partial v_y}{\partial y} - \frac{\partial v_x}{\partial x} \end{pmatrix} .$$

$\alpha_1 = 1$ and $\alpha_2 = 5/4$ in the limit $(\nu_{ii}/\omega_c)^2 << 1$ which is experimentally valid in our case. Substituting Eqs. (5), (6), and (7) into Eq. (4) and taking the x and y components respectively produces

$$\frac{\partial v_x}{\partial t} + v_{oy} \frac{\partial v_x}{\partial y} = \frac{e}{M}\left[-\frac{\partial \phi_1}{\partial x} + \frac{v_y B}{c}\right] - \frac{KT}{M}\frac{\partial}{\partial x}\left(\frac{n_1}{n_0}\right) + \frac{KT}{2\omega_c M}\frac{n_0'}{n_0}\left[\frac{\partial v_y}{\partial x} +\right.$$

$$\left. + \frac{\partial v_x}{\partial y}\right] + \frac{KT}{2\omega_c^2 M}\nu_{ii}\frac{n_0'}{n_0}\left[\frac{\partial v_x}{\partial x} - \frac{\partial v_y}{\partial y}\right] + \frac{KT}{2\omega_c M}\left[\frac{\partial^2 v_y}{\partial x^2} + \frac{\partial^2 v_y}{\partial y^2}\right] + \tag{8}$$

$$+ \frac{KT}{4\omega_c^2 M}\nu_{ii}\left[\frac{\partial^2 v_x}{\partial x^2} + \frac{\partial^2 v_x}{\partial y^2}\right]$$

for the x component and

$$\frac{\partial v_y}{\partial t} + v_{oy}\frac{\partial v_y}{\partial y} = \frac{e}{M}\left[-\frac{\partial \phi_1}{\partial y} - \frac{v_x B}{c}\right] - \frac{KT}{M}\frac{\partial}{\partial y}\left(\frac{n_1}{n_0}\right) + \frac{KT}{2M\omega_c}\frac{n_0'}{n_0}\left[\frac{\partial v_y}{\partial y} -\right.$$

$$\left. - \frac{\partial v_x}{\partial x}\right] + \frac{KT}{2\omega_c^2 M}\nu_{ii}\frac{n_0'}{n_0}\left[\frac{\partial v_y}{\partial x} + \frac{\partial v_x}{\partial y}\right] - \frac{KT}{2\omega_c M}\left[\frac{\partial^2 v_x}{\partial x^2} + \frac{\partial^2 v_x}{\partial y^2}\right] + \tag{9}$$

$$+ \frac{KT}{4\omega_c^2 M}\nu_{ii}\left[\frac{\partial^2 v_x}{\partial x^2} + \frac{\partial^2 v_y}{\partial y^2}\right]$$

for the y component. Using the assumed periodic dependence of the perturbed quantities on these equations we get

$$-i(\omega + k_y v_D)v_x = -i k_x v_{i+h}^2\left(\frac{e\phi_1}{KT} + \frac{n_1}{n_0}\right) + v_y\left[\omega_c - \frac{1}{2} i v_D k_x +\right.$$

$$\left. + \frac{1}{2} i k_y v_D \frac{\nu_{ii}}{\omega_c} - \frac{1}{2}(k_x^2 + k_y^2)\rho_i^2\omega_c\right] + i v_x\left[i\frac{(k_{ii}^2 + k_y^2)}{q}\rho_i^2\nu_{ii} - \frac{1}{2}\frac{k_{ii} v_D}{\omega_c}\nu_{ii} - \frac{1}{2} k_y v_D\right] \tag{10}$$

and

$$-i(\omega + k_y v_D) v_y = -i k_y v_{ith}^2 \left(\frac{e\phi_1}{kT} + \frac{n_1}{n_0}\right) - \nu_x \left[\omega_c - \frac{1}{2} i k_x v_D + \frac{1}{2} i k_y v_D \frac{\nu_{ii}}{\omega_c} -\right.$$

(11)

$$\left. -\frac{1}{2}(k_x^2 + k_y^2)\rho_i^2 \omega_c \right] + i v_y \left[i \frac{(k_x^2 + k_y^2)}{4} \rho_i^2 \nu_{ii} - \frac{1}{2} \frac{k_x v_D}{\omega_c} \nu_{ii} - \frac{1}{2} k_y v_D \right]$$

where $\rho_i^2 = v_{ith}^2/\omega_c^2$ the ion cyclotron radius with $v_{ith} = (kT/M)^{1/2}$, the ion thermal velocity. The following quantities are defined for convenience;

$$\Omega = \omega + k_y v_D \ , \quad b = k_\perp^2 \rho_i^2 \ , \quad k_\perp^2 = k_x^2 + k_y^2 \ ,$$

$$C = \frac{1}{2} i k_y v_D \frac{\nu_{ii}}{\omega_c} - \frac{1}{2} i k_x v_D - \frac{1}{2} b \omega_c \ ,$$

$$D = \frac{1}{4} i b \nu_{ii} - \frac{1}{2} k_x v_D \frac{\nu_{ii}}{\omega_c} - \frac{1}{2} k_y v_D \ ,$$

$$\Phi = \frac{e\phi_1}{kT} + \frac{n_1}{n_0} \ .$$

Solving Eqs. (10) and (11) for v_x and v_y gives

$$(12) \qquad v_y = -\frac{k_y v_{ith}^2}{\omega_c^2} \Phi \frac{(\Omega + D)}{(1 + 2C\omega_c^{-1})} + i \frac{k_x v_{ith}^2}{\omega_c^2} \Phi \frac{(\omega_c + C)}{(1 + 2C\omega_c^{-1})}$$

and

$$(13) \qquad v_x = -\frac{i k_y v_{ith}^2}{\omega_c^2} \Phi \frac{(\omega_c + C)}{(1 + 2C\omega_c^{-1})} - \frac{k_x v_{ith}^2}{\omega_c^2} \Phi \frac{(\Omega + D)}{(1 + 2C\omega_c^{-1})} \ .$$

In obtaining v_x and v_y we have made the approximations that (D^2/ω_c^2), $(C/\omega_c)^2$, $(\Omega/\omega_c)^2$ are all $\ll 1$ and therefore are neglected. These are quite valid experimentally. The next step is to linearize the continuity equation. This equation is just

$$\frac{\partial n}{\partial t} + \nabla\cdot(n\underline{v}) = 0$$

Linearizing and Fourier analyzing yields

$$(14)\quad -i\Omega\frac{n_1}{n_0} + ik_x v_x + ik_y v_y + v_x\frac{n_0'}{n_0} = 0 \ .$$

Substituting Eqs. (12) and (13) into Eq. (14) gives us

$$(15)\quad \Omega\frac{n_1}{n_0}\left(1 + 2C\omega_c^{-1}\right) + b\,\Phi(\Omega + D) - \frac{k_y v_D}{\omega_c}\Phi(\omega_c + C) + \\ + \frac{ik_x v_D}{\omega_c}\Phi(\Omega + D) = 0 \ .$$

For the case $k_x > n_0'/n_0$ and $\nu_{ii} < \omega_c$, the expressions for C and D can be approximated as

$$D = i\frac{1}{4}b\nu_{ii} - \frac{1}{2}k_y v_D$$

$$(16)\quad C = -\frac{1}{2}b\omega_c$$

and the last term of Eq. (15) can be dropped so that this equation is now

$$\Omega\frac{n_1}{n_0}(1-b) + b\,\Phi\left(\omega + \tfrac{1}{2}k_y v_D + i\tfrac{1}{4}b\nu_{ii}\right) - \frac{k_y v_D}{\omega_c}\Phi\left(\omega_c - \tfrac{1}{2}b\omega_c\right) = 0 \ .$$

or upon rearranging terms

$$(17)\quad \omega\frac{n_1}{n_0} - k_y v_D\frac{e\phi_1}{kT}(1-b) + b\omega\frac{e\phi_1}{kT} + i\frac{1}{t_\perp}\left(\frac{n_1}{n_0} + \frac{e\phi_1}{kT}\right) = 0$$

where $t_\perp^{-1} = 1/4(b^2\nu_{ii})$.

We next obtain an expression for the electron continuity equation. The equations of motion are

$$(18)\quad 0 = -ne\left[\underline{E}_\perp + \frac{\underline{v}_\perp \times \underline{B}}{c}\right] - \nabla_\perp P$$

for motion perpendicular to B, and

(19) $$0 = -ne E_{\parallel} - \nabla_{\parallel} p - n m_e \nu_{ei} v_{\parallel e}$$

for motion parallel to B. ν_{ei} is the electron-ion collision frequency. The zero order motion from Eq. (18) is

$$\frac{n_o e V_{oye} B}{c} + kT \frac{\partial n_o}{\partial x} = 0$$

since $\nabla_{\perp} n_o = dn_o/dx\, \hat{x}$. Thus

(20) $$V_{oye} = - c \frac{kT}{eB} \frac{n_o'}{n_o} \equiv V_D \quad .$$

Since we assume $E_{\parallel o} = \partial /\partial z = 0$ for zero order quantities, $v_{\parallel o} = 0$. For the first order motion we linearize Eqs. (18) and (19) as in the case of the ions. The x and y components are respectively

$$n_o e \frac{\partial \phi_1}{\partial x} - n_o e \frac{V_{ye} B}{c} - n_o kT \frac{\partial}{\partial x}\left(\frac{n_{1e}}{n_o}\right) = 0$$

and

$$n_o e \frac{\partial \phi_1}{\partial y} + n_o e \frac{V_{xe} B}{c} - n_o kT \frac{\partial}{\partial y}\left(\frac{n_{1e}}{n_o}\right) = 0$$

Again Fourier analyzing and solving for v_{ex} and v_{ye} we obtain

(21) $$V_{xe} = \frac{i k_y v_{ith}^2}{\omega_c}\left(\frac{n_{1e}}{n_o} - \frac{e\phi_1}{kT}\right)$$

and

(22) $$V_{ye} = -\frac{i k_x v_{ith}}{\omega_c}\left(\frac{n_{1e}}{n_o} - \frac{e\phi_1}{kT}\right)$$

For the z component we solve Eq. (19) to obtain

(23) $$V_{ze} = i K_z \frac{v_{eth}^2}{\nu_{ei}}\left(\frac{e\phi_1}{kT} - \frac{n_1}{n_o}\right)$$

where $v_{eth} = (kT/m_e)^{1/2}$, the electron thermal velocity. The linearized

electron continuity equation is

$$(24) \qquad -i\Omega_e \frac{n_{1e}}{n_o} + i\left(k_x v_{xe} + k_y v_{ye} + k_z v_{ze}\right) + v_{xe}\frac{n_o'}{n_o} = 0$$

where $\Omega_e = \omega - k_y v_D$. Substituting Eqs. (21), (22), and (23) into Eq. (24) gives us

$$(25) \quad \Omega_e \frac{n_{1e}}{n_o} + k_y v_D\left(\frac{n_{1e}}{n_o} - \frac{e\phi_1}{KT}\right) + i\frac{1}{t_{11}}\left(\frac{n_{1e}}{n_o} - \frac{e\phi_1}{KT}\right) = 0$$

or upon rearranging terms

$$(26) \quad \omega\frac{n_{1e}}{n_o} - k_y v_D\frac{e\phi_1}{KT} + i\frac{1}{t_{11}}\left(\frac{n_{1e}}{n_o} - \frac{e\phi_1}{KT}\right) = 0$$

where $t_{11}^{-1} = k_z^2 v_{eth}^2/\nu_{ei}$.

We can now obtain the dispersion relation by solving Eqs. (15) or (17) and (25) or (26) for n_1/n_o and n_{1e}/n_o respectively and equating the two expressions. We solve Eq. (25) for n_{1e}/n_o in terms of $\Phi (= e\phi/kT + n_1/n_o)$ and substitute this expression into Eq. (15). First of all $\Omega_e = \omega - k_y v_D =$ $= \Omega - 2k_y v_D$ since $\Omega = \omega + k_y v_D$. Therefore Eq. (25) becomes

$$\Omega\frac{n_{1e}}{n_o} - k_y v_D\left(\frac{e\phi_1}{KT} + \frac{n_1}{n_o}\right) + i\frac{1}{t_{11}}\left(\frac{n_{1e}}{n_o} - \frac{e\phi_1}{KT}\right) = 0$$

or rearranging and solving for n_{1e}/n_o we get

$$\frac{n_{1e}}{n_o} = \frac{k_y v_D + i\frac{1}{t_{11}}}{\Omega + 2i\frac{1}{t_{11}}}\Phi \quad .$$

Substituting into Eq. (15) yields

$$\Omega^2\left[b + i\frac{k_x v_D}{\omega_c}\right] + \Omega\left[bD + 2i\frac{1}{t_{11}}b + k_y v_D(1 + 2C\omega_c^{-1}) + \right.$$

$$(27) \quad \left. + \frac{1}{t_{11}}i\left(1 + 2C\omega_c^{-1}\right) - k_y v_D(1 + C\omega_c^{-1}) + i\frac{k_x v_D}{\omega_c}D - \frac{2}{t_{11}}\frac{k_x v_D}{\omega_c}\right] + \quad .$$

$$+\frac{2i}{t_{\parallel}}bD - k_y V_D\left(1+C\omega_c^{-1}\right)\frac{2i}{t_{\parallel}} - \frac{2}{t_{\parallel}}D\frac{k_x V_D}{\omega_c} = 0 \quad .$$

This complicated dispersion relation is greatly simplified by using the assumptions $(\nu_{\parallel}/\omega_c)$, $(k_x^{-1}\, n_o'/n_o) < 1$. This has already been done in obtaining Eq.(17). Therefore by combining Eqs. (17) and (26) as we just did for Eqs. (15) and (25) we get the dispersion relation presented in the text,

$$(28)\quad \omega^2 b + \omega\left[k_y V_D b + i\left\{\frac{1}{t_{\parallel}}(1+b)+\frac{1}{t_{\perp}}\right\}\right] - i k_y V_D\left[\frac{1}{t_{\parallel}}(1-b)-\frac{1}{t_{\perp}}\right] - \frac{2}{t_{\parallel}t_{\perp}} = 0$$

We can solve this equation in several limits by expanding the square root. First,

$$2b\omega = -\left[k_y V_D b + i\left(\frac{1}{t_{\parallel}}(1+b)+\frac{1}{t_{\perp}}\right)\right] \pm \left\{\left[b k_y V_D + i\left(\frac{1}{t_{\parallel}}(1+b)+\frac{1}{t_{\perp}}\right)\right]^2 + 4b i k_y V_D\left[\frac{1}{t_{\parallel}}(1-b)-\frac{1}{t_{\perp}}\right] + \frac{8b}{t_{\parallel}t_{\perp}}\right\}^{1/2}$$

or

$$2b\omega = -\left[k_y V_D b + i\left(\frac{1}{t_{\parallel}}(1+b)+\frac{1}{t_{\perp}}\right)\right] \pm \left\{(k_y V_D b)^2 - \left(\frac{1}{t_{\parallel}}(1+b)+\frac{1}{t_{\perp}}\right)^2 + \frac{8b}{t_{\perp}t_{\parallel}} + i\left[2 k_y V_D b\left(\frac{3}{t_{\parallel}}\left(1-\frac{1}{3}b\right)-\frac{1}{t_{\perp}}\right)\right]\right\}^{1/2} .$$

Factoring out the real part of the radical and assuming

$$\left(\frac{1}{t_{\parallel}}(1+b)+\frac{1}{t_{\perp}}\right)^2 \equiv A^2 > (k_y V_D)^2 b^2 + \frac{8b}{t_{\perp}t_{\parallel}}$$

we can write

$$2b\omega = -\left[k_y V_D b + i\left(\frac{1}{t_{\parallel}}(1+b)+\frac{1}{t_{\perp}}\right)\right] \pm i A\left[1 - \frac{(k_y V_D b)^2 + \frac{8b}{t_{\perp}t_{\parallel}}}{A^2}\right]^{1/2} \times \left\{1 - \frac{2ib\left[k_y V_D\left(\frac{3}{t_{\parallel}}\left(1-\frac{1}{3}b\right)-\frac{1}{t_{\perp}}\right)\right]}{A^2}\right\}^{1/2}$$

or again with the assumption we can expand the square roots to obtain

$$2b\omega = -\left[k_y v_D b + i\left(\frac{1}{t_{11}}(1+b)+\frac{1}{t_\perp}\right)\right] \pm iA\left[1-\frac{(k_y v_D b)^2+\frac{8b}{t_{11}t_\perp}}{2A^2}\right]\times$$

$$(29)\qquad \times\left\{1-\frac{ib\left[k_y v_D\left(\frac{3}{t_{11}}(1-\frac{1}{3}b)-\frac{1}{t_\perp}\right)\right]}{A^2}+\frac{b^2\left[\frac{9}{t_{11}^2}(1-\frac{2}{3}b+\frac{1}{9}b^2)-\frac{6}{t_{11}t_\perp}(1-\frac{1}{2}b)+\frac{1}{t_\perp^2}\right]}{2A^4}\right\}.$$

The assumption implies that $(t_{11})^{-2} > (k_y v_D b)^2$. Since we are to obtain expressions valid for $t_{11}^{-1} \ll k_y v_D$ and $\gg k_y v_D$ this necessarily limits the value of b so that $(t_{11})^{-2} > (k_y v_D b)^2$. Our experimental conditions show that $t_{11}^{-1} \simeq k_y v_D$ so that the assumption allowing the expansion is quite valid. We now can write down expressions for ω_R and ω_g from Eq. (29) as

$$2b\omega_R = -k_y v_D + \frac{k_y v_D\left(\frac{3}{t_{11}}(1-\frac{1}{3}b)-\frac{1}{t_\perp}\right)}{A}$$

or

$$(30)\qquad \omega_R = \frac{k_y v_D\left[1-b-t_{11}/t_\perp\right]}{\left[1+b+t_{11}/t_\perp\right]}$$

and

$$2b\omega_g = \frac{\frac{-8b}{t_{11}t_\perp}-(k_y v_D b)^2}{A}+\frac{(k_y v_D b)^2\left[\frac{9}{t_{11}^2}(1-\frac{2}{3}b+\frac{1}{9}b^2)-\frac{6}{t_{11}t_\perp}(1-\frac{1}{3}b)+\frac{1}{t_\perp^2}\right]}{A^2}$$

or

$$(31)\qquad \omega_g = \frac{2(k_y v_D)^2 b\, t_{11}}{(1+b+t_{11}/t_\perp)}\left[\frac{(1-b-t_{11}/t_\perp)}{(1+b+t_{11}/t_\perp)^2}-\frac{1}{b(k_y v_D)^2 t_\perp t_{11}}\right].$$

In the limit $t_\perp \to \infty$ and $b \ll 1$ we get

$$\omega_R = k_y v_D \quad , \quad \omega_g = 2(k_y v_D)^2 b t_{\parallel}$$

and no stabilizing effect is predicted. For small $t_{\parallel}$ such that $t_{\parallel}^{-1} \gg k_y v_D$ and therefore $t_{\parallel} \ll t_{\perp}$, the terms $t_{\parallel}/t_{\perp}$ in Eq. (31) can be dropped. If we further make the assumption $b \ll 1$ then Eq. (31) can be written as

$$\omega_g = 2(k_y v_D)^2 b t_{\parallel} \left[1 - \frac{1}{b(k_y v_D)^2 t_{\perp} t_{\parallel}} \right] . \tag{32}$$

Stability is achieved when $[b(k_y v_D)^2 t_{\parallel}] = t_{\perp}^{-1}$. Finally in the case of large $t_{\parallel}$ such that $t_{\parallel}^{-1} \ll k_y v_D$ the last term in Eq. (31) can be neglected and the expression for ω_g becomes

$$\omega_g = \frac{2(k_y v_D)^2 b t_{\parallel}}{(1 + b + t_{\parallel}/t_{\perp})^3} \left[1 - b - \frac{t_{\parallel}}{t_{\perp}} \right] \tag{33}$$

and stability comes about when $t_{\parallel} = t_{\perp}(1-b)$.